Computer Modeling in Engineering & Sciences

Tech Science Press

Doi:10.32604/cmes.2025.064854

REVIEW

Advances in Crack Formation Mechanisms, Evaluation Models, and Compositional Strategies for Additively Manufactured Nickel-Based Superalloys

Huabo Wu[1,2], **Jialiao Zhou**[3], **Lan Huang**[1,2,*], **Zi Wang**[1,2,*], **Liming Tan**[1,2], **Jin Lv**[4] **and Feng Liu**[1,2]

[1]State Key Laboratory of Powder Metallurgy, Central South University, Changsha, 410083, China
[2]Research Institute of Powder Metallurgy, Central South University, Changsha, 410083, China
[3]Hunan Runfeng Innovation Tech Co., Ltd., Zhuzhou, 412007, China
[4]Puli (Ningbo) Advanced Material Technology Co., Ltd., Ningbo, 315599, China

*Corresponding Authors: Lan Huang. Email: lhuang@csu.edu.cn; Zi Wang. Email: wangzi@csu.edu.cn

Received: 25 February 2025; Accepted: 04 June 2025; Published: 30 June 2025

ABSTRACT: Nickel-based superalloys are indispensable for high-temperature engineering applications, yet their additive manufacturing (AM) is plagued by significant cracking defects. This review investigates crack failure mechanisms in AM nickel-based superalloys, emphasizing methodologies to evaluate crack sensitivity and compositional design strategies to mitigate defects. Key crack types—solidification, liquation, solid-state, stress corrosion, fatigue, and creep-fatigue cracks—are analyzed, with focus on formation mechanisms driven by thermal gradients, solute segregation, and microstructural heterogeneities. Evaluation frameworks such as the Rappaz-Drezet-Gremaud (RDG) criterion, Solidification Cracking Index (SCI), and Strain Age Cracking (SAC) index are reviewed for predicting crack susceptibility through integration of thermodynamic parameters, solidification kinetics, and mechanical properties. Alloy compositional design strategies are presented, including optimization of strengthening elements (Al, Ti), grain boundary modifiers (B, Zr, Re), and impurity control (C, O), which suppress crack initiation and propagation via microstructure refinement and enhanced high-temperature resistance. Computational approaches, such as thermodynamically assisted design, high-throughput experimentation, and machine learning, are highlighted for decoding complex composition-structure-property relationships. Challenges in modeling multi-scale defect interactions and developing unified frameworks for manufacturing- and service-induced cracks are outlined. This review underscores the necessity of integrated computational-experimental strategies to advance reliable AM of nickel-based superalloys, providing insights for defect prediction, alloy optimization, and process control.

KEYWORDS: Additive manufacturing; nickel-based superalloys; cracking; failure mechanism; composition design

1 Introduction

With the rapid advancement of modern industry, the demand for high-performance materials in aviation, aerospace, energy, and high-temperature industrial equipment is steadily increasing [1–3]. Among these materials, nickel-based superalloys have emerged as critical candidates for the fabrication of high-temperature components owing to their exceptional performance at elevated temperatures, as well as their superior oxidation and corrosion resistance [4,5]. Evolving from their initial application in simple components to the production of complex, precision-engineered, high-performance parts today, nickel-based superalloys have been indispensable to technological progress [6,7]. Although conventional manufacturing processes have historically dominated the production of nickel-based superalloy components, they exhibit significant limitations when it comes to fabricating high-performance parts with intricate geometries [8–10].

Copyright © 2025 The Authors. Published by Tech Science Press.
This work is licensed under a Creative Commons Attribution 4.0 International License, which permits unrestricted use, distribution, and reproduction in any medium, provided the original work is properly cited.

Against this backdrop, additive manufacturing technologies have rapidly emerged. Techniques like Laser Powder Bed Fusion (LPBF) and Wire Arc Additive Manufacturing (WAAM) have increasingly become pivotal for fabricating nickel-based superalloy components, owing to their remarkable design flexibility, minimal material waste, and high machining precision [11–13]. Moreover, additive manufacturing not only facilitates the precise fabrication of intricate geometries but also offers a novel design space for optimizing alloy compositions and controlling microstructures, thereby advancing the state-of-the-art in nickel-based superalloy component production [14,15].

However, additive manufacturing technologies encounter several challenges in fabricating nickel-based superalloy components. Chief among these challenges are failure phenomena—most notably cracking—which significantly undermine the performance and reliability of additively manufactured nickel-based superalloy components. Such failures not only compromise the aesthetic quality and dimensional accuracy of the components but also pose potential safety hazards during operation [16–20]. To address these issues, researchers have developed various failure models rooted in numerical simulations and experimental investigations of the additive manufacturing process that are capable of predicting failure phenomena such as cracking [21,22]. In-depth analysis of these models facilitates a more comprehensive understanding of the mechanisms driving crack formation. Concurrently, alloy compositional design is being explored as a strategy to mitigate cracking by optimizing compositions to enhance high-temperature performance and crack resistance [23,24].

Alloy composition design is a critical determinant of the properties of nickel-based superalloys; in additive manufacturing, it directly governs microstructural evolution as well as the initiation and propagation of defects [25–27]. During additive manufacturing, nickel-based superalloys frequently exhibit solid-solution segregation, grain boundary weakening, and thermal cracking, with these defects being intimately linked to the alloy's chemical composition [28,29]. Optimizing alloy composition boosts high-temperature strength, oxidation resistance, and corrosion resistance whilst simultaneously curbing crack initiation and propagation. Furthermore, implementing targeted design strategies to mitigate typical additive manufacturing defects such as porosity and residual stresses is pivotal to enhancing the reliability and extending the service life of the nickel-based superalloys. The rapid cooling, localized high temperatures, and steep temperature gradients characteristic of additive manufacturing often result in inhomogeneous compositional distributions, subsequently giving rise to defects such as solidification, liquefaction, and solid-state cracks [30,31]. Thus, precise compositional design to control phase composition, crystal structure, and microstructural homogeneity is pivotal in addressing failure issues in nickel-based superalloys during additive manufacturing [32,33]. While most current studies concentrate on compositional design in traditional manufacturing, a significant research gap persists regarding compositional optimization in additive manufacturing processes.

While extensive research has focused on the compositional design and failure mechanisms of nickel-based superalloys, studies addressing the compositional control of defects unique to additive manufacturing remain limited [34]. In particular, targeted research on improving crack resistance and high-temperature reliability is scarce. This review aims to comprehensively analyze the crack failure mechanisms in additively manufactured nickel-based superalloys and explore how tailored compositional design can mitigate these failure issues, particularly those associated with additive manufacturing. By implementing optimized design strategies, this review seeks to enhance alloy performance and reliability. Moreover, by critically reviewing current literature, this paper identifies the limitations of existing compositional designs and offers valuable insights for future research directions.

2 Crack Types in Additively Manufactured NICKEL-Based Superalloys and Evaluation of Crack Sensitivity

2.1 Manufacturing Process Cracks

2.1.1 Solidification Cracks

Solidification cracking is a prevalent defect in additive manufacturing, particularly in laser powder bed fusion and arc additive manufacturing of nickel-based superalloys. The rapid cooling of localized molten pools and steep thermal gradients in these processes complicates the crack formation mechanisms [35,36]. During the solidification of alloys, the formation of liquid films is the primary cause of crack development. This phenomenon, characterized by grain boundary segregation and the precipitation of low-melting phases, creates uneven stress distribution during solidification, ultimately triggering crack formation.

Fig. 1 illustrates the mechanism of solidification crack formation in metal additive manufacturing. Initially, rapid cooling induces the formation of a dendritic structure. Concurrently, solute elements such as Al and Ti segregate at the dendrite boundaries, creating a low-melting-point liquid film that promotes crack initiation. As the dendritic arms interconnect, the liquid metal fragments into isolated regions that cannot be replenished, leading to the formation of micro-defects. Additionally, solidification shrinkage and thermal stresses accumulate between the dendrites. When these stresses surpass the load-bearing capacity of the liquid film, cracks propagate preferentially along these weakened regions, eventually forming penetrating cracks [31]. This process demonstrates that the synergistic effect of solute segregation and stress is the primary mechanism driving crack initiation and propagation, thereby providing a theoretical basis for process optimization.

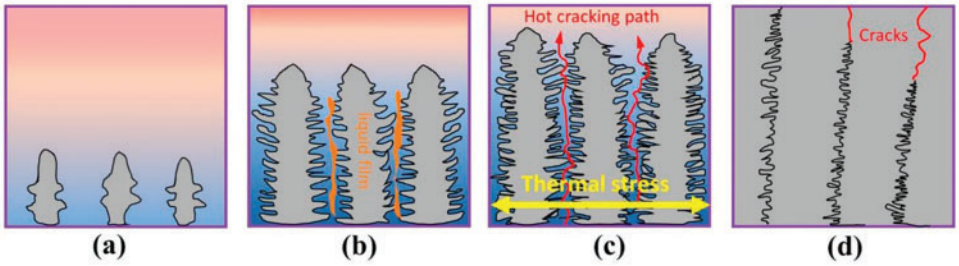

Figure 1: Schematic showing the formation mechanism of solidification cracking. (a) Formation of dendrites at the interface between molten and solid metal phases during rapid heating and cooling in metal AM processes. (b) Segregation of solute elements leads to the formation of liquid films enriched in solute elements between growing dendrite arms. (c) Accumulation of thermal stress in liquid films causes the initiation of hot cracking paths during solidification. (d) Propagation of cracks along the cracking paths in the final stage of solidification results in the formation of cracks in the solidified material [31]

The precipitation of low-melting-point phases significantly contributes to solidification cracking. In additive manufacturing, rapid solidification and localized supersaturation can induce the formation and accumulation of these phases, thereby degrading the material's mechanical properties. Their enrichment at grain boundaries exacerbates embrittlement, increasing the material's susceptibility to stress-induced solidification cracking.

Specifically, the formation of solidification cracks is strongly influenced by the chemical composition of nickel-based superalloys. Hu et al. [37] investigated the effect of titanium (Ti) addition on cracking susceptibility and microhardness in Inconel 625 during laser solid-state molding. Their findings confirmed a direct link between alloy composition and the occurrence of solidification cracks. An increase in Ti

content led to a reduced crack rate and enhanced microhardness, primarily due to a narrowed solidification temperature range and the promotion of the (γ + Laves) eutectic phase, both of which contribute to crack suppression. Furthermore, alloy composition design and elemental ratios are critical in mitigating solidification cracking. A well-controlled alloy composition and optimized compositional gradient can significantly suppress the precipitation of low-melting-point phases, thereby lowering the likelihood of solidification cracking.

In specific additive manufacturing applications, solidification cracks can severely degrade the strength and toughness of components, thereby compromising their service performance. For instance, in turbine blades used in aero-engines and gas turbines, these cracks diminish fatigue life, accelerate crack propagation, and pose a serious risk to structural integrity. Therefore, a thorough understanding of the mechanisms behind solidification crack formation and their manifestation during additive manufacturing is essential to improving the performance and reliability of nickel-based superalloys. Strategies such as optimizing alloy composition, controlling cooling rates and process parameters, and implementing appropriate post-treatment techniques can effectively suppress crack formation and enhance the quality and structural stability of additively manufactured superalloys. Kadoi et al. [38] examined the susceptibility of alloy 718 to solidification cracking in additive manufacturing using a novel horizontal tensile-type thermal cracking test. Their experiments demonstrated that both laser power and initial tensile stress significantly influence crack formation. Notably, higher laser power reduces the critical stress required to initiate cracking. Using thermoelastic–plastic analysis, the critical strain rate (CST) for solidification cracking was determined. The results revealed that higher laser power, associated with increased CST, exacerbates crack sensitivity. These findings suggest that lowering laser power is an effective strategy for mitigating solidification cracking in alloy 718 during additive manufacturing.

2.1.2 Liquation Cracking

Liquation cracking is a common failure mode in additive manufacturing, typically occurring during the cooling stage of the molten pool, driven by localized melting and solute segregation. It arises from localized melting and segregation of alloying elements, which leads to crack formation in the early stages of solidification. The onset of liquation cracking is strongly influenced by the thermal gradient of the molten pool, the cooling rate, and the spatial distribution of alloying elements. Studies have shown that steep temperature gradients and rapid cooling within the melt pool can induce localized melting, particularly in regions enriched with low-melting-point phases or alloying elements [39]. These regions typically exhibit unstable liquid-solid interfaces, where localized stress concentrations promote the initiation of liquation cracks. For instance, γ-γ' eutectic phases have been observed to remelt along grain boundaries, forming liquid films that facilitate liquation crack propagation [40,41]. Additionally, Li et al. [42] studied liquation cracking mechanisms in the high γ' content nickel-based superalloy K4002, processed via Electron Beam Powder Bed Fusion (EBPBF). Their findings indicated that liquation cracking is the dominant failure mode, driven by stray-grain chains that create high-angle grain boundaries, elevated geometrically necessary dislocation densities, restricted dislocation mobility due to $Cr_{23}C_6$ carbides, and localized low-melting-point regions. Carbides, particularly MC and M_6C types, play a key role in liquation cracking susceptibility. Fig. 2 illustrates the metallurgical mechanism responsible for the broadening of the Liquation Cracking Temperature Range (LCTR) during repair welding of 247LC superalloys subjected to prolonged high-temperature exposure. Extended high-temperature exposure promotes the precipitation of MC and M_6C carbides, whose liquation onset temperatures fall below the alloy's solidus. This condition favors localized melting during welding, triggering liquation crack formation. As exposure duration increases, the volume fraction of these carbides rises, thereby significantly widening the LCTR [43].

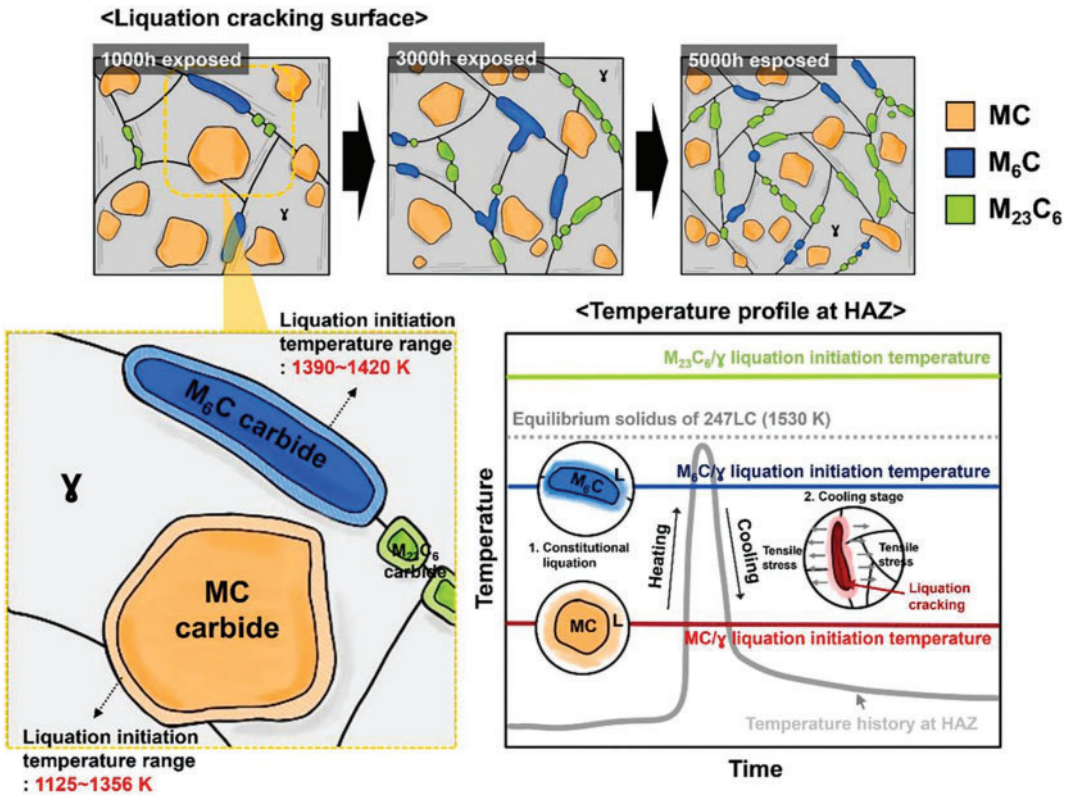

Figure 2: Summarization of the welding metallurgical mechanism of LCTR enlargement for long-term-serviced 247LC superalloy repair welds [43]

Liquation cracking has also been linked to the presence of the Laves phase. Chen et al. [44] investigated the influence of substrate cooling on microstructure evolution and liquation cracking behavior during laser additive manufacturing of IN718 superalloy. The researchers found that liquation cracking mainly stems from the remelting of low-melting-point Laves phase particles in the heat-affected zone (HAZ). This process is accompanied by the creation of eutectic liquid films at grain boundaries and localized stress concentrations during final solidification. Poor grain boundary orientation was identified as the critical factor. Specifically, large-angle grain boundaries (>15°) exacerbate stress concentrations because of the high thermal stability of the intergranular liquid film. Enhanced substrate cooling promotes the formation of columnar grains and reduces the prevalence of large-angle grain boundaries, thereby effectively mitigating liquation cracking. This study offers a microstructural basis for defect suppression in laser-based additive manufacturing of superalloys and suggests a viable pathway for active control of liquation cracking through process optimization. Luu et al. [45] explored strategies to mitigate liquation cracking in selective laser melting of Inconel 718 by adjusting layer thickness and laser energy density. They found that while laser energy density influenced dendritic growth, layer thickness had a more pronounced impact on liquation crack susceptibility. Crack formation was effectively suppressed by reducing the layer thickness to 40 μm, which promoted favorable transformations in Laves phase morphology and grain boundary structure, ultimately enhancing the mechanical performance of the alloy.

Liquation cracking significantly compromises the mechanical properties and service life of additively manufactured nickel-based superalloys. This issue is particularly critical in aerospace and other high-performance applications, where liquation cracking reduces tensile strength and fatigue life, while also

accelerating crack propagation and threatening structural integrity. Mitigating liquation cracking requires a multifaceted strategy. This includes optimizing alloy composition, particularly by minimizing the segregation of low-melting-point elements, and employing tailored process parameters and cooling strategies to suppress crack initiation and propagation. Additionally, post-processing heat treatment can refine the alloy's microstructure, thereby improving both crack resistance and high-temperature performance [46].

2.1.3 Solid-State Cracks

Solid-state cracks typically arise due to thermal effects associated with the additive manufacturing process. These cracks are also referred to as high-temperature loss-of-plasticity cracks or strain-aging cracks [47,48]. Unlike other types of cracking, solid-state cracks commonly form during solidification and are closely linked to the crystallization behavior of the metal. Specifically, rapid cooling of the melt pool can lead to inhomogeneous solidification of grains and phases in nickel-based superalloys. This promotes stress concentration at grain boundaries, thereby facilitating crack initiation. Moreover, the formation of solid-state cracks is influenced by solid-solution strengthening elements and the characteristics of their corresponding precipitates. Excessively high or low concentrations of these elements may destabilize the solid solution, resulting in elevated localized stresses and increased crack susceptibility.

2.2 Service Environment Cracks

2.2.1 Stress Corrosion Cracking

Stress corrosion cracking (SCC) refers to the propagation of cracks in materials exposed to both mechanical stress and corrosive environments at elevated temperatures [49–51]. It typically occurs when external or internal stresses act on a material concurrently exposed to a corrosive medium such as water vapor, acidic solutions, or saline environments [52]. Crack initiation occurs when the corrosive medium reacts with the material surface, locally degrading toughness and enabling crack propagation under applied stress. In the early stages, crack growth is often subcritical and difficult to detect. However, once the crack reaches a critical size, it can cause brittle fracture or catastrophic failure. A schematic illustration of stress corrosion cracking in a superalloy is presented in Fig. 3.

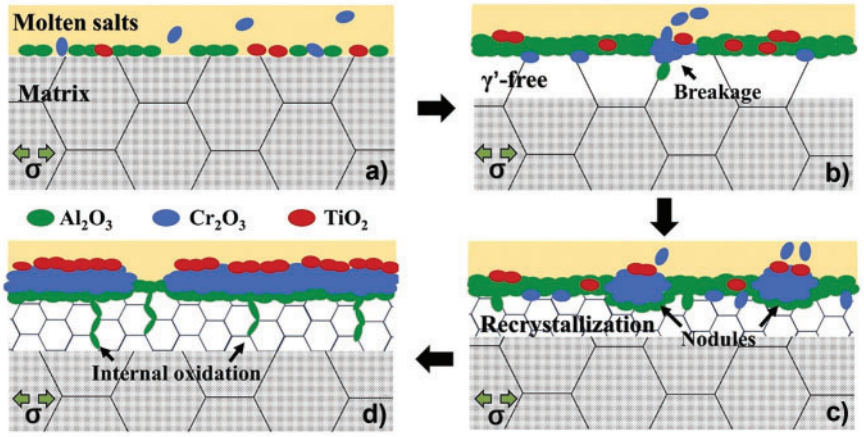

Figure 3: Schematic representation of the organisational evolution and corrosion product formation of superalloys in a fireside corrosion environment with high creep stresses. (a) Formation of oxides and Dissolution of Cr_2O_3. (b) Breakages on Al_2O_3 scale and Formation of γ'-free zone. (c) Nodules coarsen into each other and Internal oxidation along GBs. (d) Recrystallization in γ'-free zone and Formation of nodular products [53]

During additive manufacturing, nickel-based superalloys are frequently deployed in complex service environments, particularly in high-temperature and high-pressure systems such as aero-engines, nuclear reactors, and gas turbines. In such conditions, the synergistic effects of mechanical stress and corrosive media can induce stress corrosion cracking in the alloy [54]. These aggressive environments can significantly accelerate crack initiation and propagation due to the interaction between high-temperature stress and corrosive species, thereby compromising the structural integrity and service lifespan of the material.

In recent years, several researchers have conducted simulation studies on stress corrosion cracking (SCC) in nickel-based superalloys. Nguyen et al. [55] examined SCC propagation in Inconel 600 when exposed to an acidified thiosulfate environment. They created a novel multiphysics model using a phase-field framework. This model incorporated Digital Image Correlation (DIC) and diffusion coefficients from first-principles calculations. It effectively simulated environment-assisted cracking, including crack interaction and shielding effects, with results aligning well with experimental data. Sato et al. [56] developed a simulation code to evaluate SCC behavior in Inconel 600 under complex stress/strain conditions. The model employs finite element analysis to calculate the stress and strain fields near the crack tip and integrates a kinetic formulation of crack-tip reactions to predict crack growth rates in specific corrosive environments. Arnoux [57] explored the atomic-scale mechanisms of SCC in stainless steel and nickel alloys used in pressurized water reactors. Molecular statics simulations revealed that hydrogen accumulation at grain boundaries promotes brittle fracture at the crack tip. Based on these findings, a theoretical model was proposed to explain irradiation-assisted stress corrosion cracking (IASCC), and its predictions were validated against experimental data.

Additionally, Bale et al. [58] leveraged deep learning-enhanced X-ray microscopy to analyze stress corrosion cracking in CMSX-4 turbine blade superalloys. By combining high-resolution X-ray imaging with deep learning algorithms for data reconstruction and segmentation, and integrating these with Focused Ion Beam/Scanning Electron Microscope (FIB-SEM) and electron microscopy techniques, they performed a detailed three-dimensional quantitative analysis of thermally induced damage. The study examined microstructural features such as porosity, surface crack morphology, dendrite orientation, and their influence on damage propagation. The proposed correlation workflow effectively identified structural defects that are typically undetectable using conventional microscopy. These findings offer critical insights into the damage mechanisms associated with thermal corrosion, providing a valuable scientific foundation for addressing blade root cracking and improving the service life of structural components.

Stress corrosion cracking (SCC) degrades the mechanical properties and long-term durability of additively manufactured nickel-based superalloys and poses a significant risk to their structural integrity under extreme service conditions [59]. Addressing this issue requires minimizing stress concentration through compositional optimization, alongside enhanced control and isolation of corrosive environments. A combination of optimized alloy design, application of high-temperature protective coatings, and refinement of manufacturing parameters can effectively suppress SCC initiation and propagation, thereby enhancing high-temperature service reliability.

2.2.2 Fatigue Crack

Fatigue cracks develop progressively in materials subjected to cyclic loading and are frequently observed in additively manufactured nickel-based superalloys, particularly under high-temperature service conditions [60–62]. Their initiation is typically associated with pre-existing microscopic defects. These defects accumulate strain during repeated loading cycles, ultimately resulting in crack nucleation and growth [63]. The formation mechanisms are multifaceted and involve defect initiation, local stress concentration, and

subsequent crack propagation. Notably, the intrinsic defects produced during additive manufacturing substantially increase the material's susceptibility to fatigue cracking.

The propagation of cracks is strongly influenced by the alloy's microstructure. In nickel-based superalloys, reinforcing phases such as the γ' phase generally contribute to enhanced mechanical strength; however, they can also promote crack propagation under certain conditions [64]. Although γ' phase precipitation improves hardness and high-temperature strength, the interface between the γ' precipitates and the matrix may serve as a preferential path for crack growth when the material is subjected to stress. This behavior is primarily attributed to the relatively weak interfacial bonding between the γ' phase and the matrix, which facilitates crack advancement, particularly under cyclic fatigue loading.

To effectively inhibit fatigue crack initiation and propagation, it is crucial to minimize the formation of microscopic defects at the source and optimize the alloy's compositional design to enhance the material's microstructure [65]. Controlling the cooling rate, residual stress, and reinforcing phase precipitation during additive manufacturing can reduce the sources of crack initiation and improve the material's fatigue properties. These optimizations significantly enhance the fatigue resistance and service life of additively manufactured nickel-based superalloys.

2.2.3 Creep-Fatigue Cracking

Creep-fatigue cracking is a prevalent failure mode in nickel-based superalloys under high-temperature service conditions. It typically occurs in environments where the material is exposed to both sustained high temperatures and cyclic loading [66,67]. At elevated temperatures, creep results from prolonged exposure to stress, causing the material to gradually deform and accumulate damage over time [68]. Additionally, fatigue is induced when the material experiences fluctuating external loads, leading to the formation of periodic microcracks.

Creep and fatigue are distinct failure mechanisms; however, in high-temperature environments, they often occur concurrently, amplifying material damage [69,70]. During creep, the material deforms slowly at elevated temperatures, causing grain boundary slip, dislocation motion, and changes in reinforcing phases. In contrast, fatigue results in localized plastic deformation under cyclic loading [71]. The interaction between the two mechanisms causes the creep effect to gradually expand microcracks, providing a foundation for fatigue crack formation. Simultaneously, the propagation of fatigue cracks accelerates creep damage accumulation, leading to a complex crack network. Additionally, studies on the creep-fatigue cracking behavior of nickel-based single-crystal superalloys in different orientations have shown that [111]-oriented specimens exhibit the longest life, while [011]-oriented specimens display the shortest life. Crack formation was primarily attributed to the formation and growth of microscopic voids [72].

To minimize creep-fatigue cracking, alloy compositional design must prioritize enhancing both high-temperature strength and fatigue resistance. The precipitation behavior of reinforcing phases, the stability of grain boundaries, and microstructural homogeneity are crucial for suppressing creep-fatigue cracking. Optimizing the content of reinforcing elements in the alloy increases γ' phase precipitation, thereby enhancing both high-temperature strength and creep resistance. Furthermore, adjusting the alloy's grain size and improving its heat treatment process can further enhance fatigue performance and reduce crack initiation and propagation.

3 Crack Evaluation Models and Criteria

Crack sensitivity evaluation is critical for understanding and mitigating defects in additively manufactured nickel-based superalloys. Various models have been developed to predict and assess crack susceptibility

based on thermodynamic parameters, solidification kinetics, and mechanical properties. These models provide valuable insights into the interplay between alloy composition, processing parameters, and crack formation mechanisms. Table 1 summarizes the crack sensitivity evaluation models used in the references.

Table 1: Crack sensitivity evaluation models summary

Model name	Formula	Scope of application	References
Solidification Cracking Index (SCI)	$SCI = \left\lvert \frac{dT}{d\left(f_s^{1/2}\right)} \right\rvert_{f_s^{1/2} \approx 1}$	Solidification cracking in AM	[73]
Freezing range (FR)	$FR = T_{Liquidus} - T_{olidus}$	Hot tearing susceptibility in casting and AM	[74]
Strain Age Cracking (SAC) Index	$SAC = \frac{dV_{\gamma'}}{dT}$	Strain-age cracking during heat treatment	[75]
Crack Sensitivity Coefficient (CSC)	$CSC = \frac{t_{f_s=0.99} - t_{f_s=0.90}}{t_{f_s=0.90} - t_{f_s=0.40}} \approx \frac{T_{f_s=0.99} - T_{f_s=0.90}}{T_{f_s=0.90} - T_{f_s=0.40}}$	Thermal tearing risk during rapid solidification in AM	[76]
Solid-state Cracking Criterion (M_{sac})	$M_{sac} = W_{Al} + 0.5W_{Ti} + 0.3W_{Nb} + 0.15W_{Ta}$	Strain-age cracking in thermal cycles	[77,78]
SAC Risk Factor (RF)	$FR = T_{Liquidus} - T_{olidus}$	Quantitative prediction of SAC behavior	[79]
Thermal Shock Resistance (TSR)	$R_{SAC} = -\frac{\nu^{\gamma'} \cdot \Delta}{T_{low}}$	Microcrack formation during SLM	[80]
Generalised hot cracking criterion	$\frac{d\varepsilon_{local}}{dt} > \left[\frac{\sqrt{1-\beta}}{2} \cdot \left\lvert \frac{d\sqrt{f_s}}{dT} \right\rvert \cdot \left(1 + \frac{1}{cos\theta}\right) \cdot \lvert CR \rvert - \frac{tan\theta}{\varphi} \cdot \frac{\lvert CR \rvert}{G} \right] + \frac{d}{dz} \left[\frac{1}{2} \left(1 - \sqrt{1-\beta} \cdot \sqrt{f_s}\right) \cdot \left(1 + \frac{1}{cos\theta}\right) \cdot \nu_z \right]_z$	Hot cracking in AM	[81]

3.1 RDG Guidelines

M. Rappaz, J.-M. Drezet, and M. Gremaud developed the Rappaz-Drezet-Gremaud (RDG) criterion to elucidate the mechanism of hot crack formation in metallic alloys during solidification. Their model accounts for solid mass deformation perpendicular to dendritic growth and the associated liquid feeding between dendrite arms, derived from the mass balance between liquid and solid phases. Based on this, they introduced a critical deformation rate $\left(\dot{\varepsilon}_{p,\max}^{-1}\right)$, above which cavitation—initiating as void nucleation—can occur. Additionally, the guideline incorporates the Heat Cracking Sensitivity (HCS) index, proposed by Clyne and Davis, to assess the susceptibility of alloys to hot cracking during solidification [82–84]. Overall, the RDG criterion serves as a predictive framework for evaluating the hot cracking tendency of alloys under solidification conditions.

(1) Prediction of Hot Crack Formation: The RDG criterion enables the prediction of hot cracking in metallic alloys under defined solidification conditions by calculating the critical deformation rate $\left(\dot{\varepsilon}_{p,\max}^{-1}\right)$. If the actual deformation rate surpasses this threshold, the nucleation of cavities may occur, initiating hot cracking.

(2) Evaluation of Hot Cracking Susceptibility: The Heat Cracking Sensitivity (HCS) index provides a quantitative measure of an alloy's tendency to undergo hot cracking under various compositional and solidification scenarios. A higher HCS index indicates increased susceptibility to hot cracking.

(3) Alloy and Process Optimization: The RDG framework enables the identification of critical alloy compositions and solidification parameters, such as cooling rate and thermal gradient, that contribute to hot cracking. This predictive capability facilitates the optimization of alloy design and processing routes to minimize hot crack formation during solidification.

3.2 Solidification Cracking Index (SCI)

The occurrence of cracking during alloy solidification is primarily governed by the processes at the grain boundaries—specifically, the feeding of the liquid phase, the growth of grains, and the accumulation of strain. In his study, Kou [73] established a cracking criterion by focusing on the interaction between liquid feeding at the grain boundaries and the growth of columnar dendrites. As shown in Fig. 4, which illustrates the physical meaning of the Kou indicator, the analysis is based on the relationship between the characteristic grain radius and the solid phase fraction (f_s).

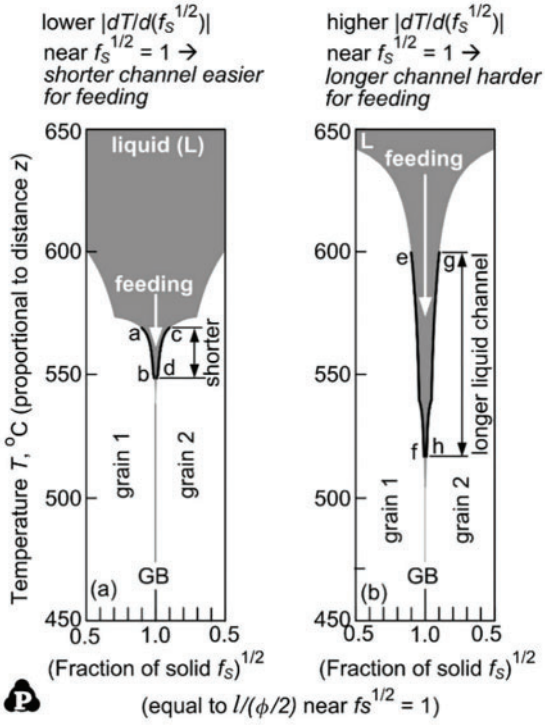

Figure 4: Physical meaning of kou indicator [73]

The Solidification Cracking Index (SCI) is defined based on the slope of the temperature versus the square root of the solid phase fraction, which is expressed as follows:

$$SCI = \left| \frac{dT}{d\left(f_s^{1/2}\right)} \right|_{f_s^{1/2} \approx 1} \tag{1}$$

where $\frac{dT}{d\left(f_s^{1/2}\right)}$ is the slope between the temperature and the square root of the solid phase fraction. A steeper slope indicates a higher resistance to grain growth and a longer liquid channel at the grain boundary. Consequently, this increases the difficulty of liquid phase feeding and thereby elevates the risk of cracking. In practical terms, a higher SCI value correlates with a greater tendency for solidification cracking. This index can be used as a predictive tool for material selection, design optimization, and process control.

Zhang et al. [85] investigated the use of SCI to assess the cracking tendency of René 104 and René 104ScY alloys. By calculating the value of $\frac{dT}{d\left(f_s^{1/2}\right)}$ for both alloys in the range of solid phase fractions f_s of 0.81 < f_s < 0.98, they found that this value was significantly lower for the René 104ScY alloy than for the René 104 alloy, suggesting that the addition of the elements Sc and Y significantly reduced the cracking tendency of the the cracking tendency of the alloy. In addition, they analysed the liquid and solid phase line temperatures of the two alloys and found that the René 104ScY alloy had a higher initial solidification temperature and a smaller range of solidification temperatures, which also contributed to the reduction of its cracking tendency. In addition, SCI can also be used to optimize process parameters such as cooling rate and strain rate, thus effectively reducing the risk of cracking [86].

3.3 Freezing Range (FR)

A series of criteria has been developed to quantify susceptibility to thermal tear cracking, emphasizing the mechanism of crack formation during solidification. The Solidification Range (FR) is a key parameter used in the model to assess cracking tendency. It was initially proposed in foundry literature as a measure of susceptibility [74]. FR is defined by calculating the temperature difference between the liquidus and solidus lines. The formula is as follows:

$$FR = T_{Liquidus} - T_{olidus} \tag{2}$$

The solid phase line is set to the temperature corresponding to a 0.99 mol fraction of solid. This model assumes complete mixing in the liquid phase and no diffusion in the solid phase, which is justified by the extremely fast cooling rates during solidification and the absence of rapidly diffusing elements in the alloy. Using a 1 K temperature step for the solidification profile, the model effectively predicts the crack susceptibility of the alloy during solidification.

3.4 Strain Age Cracking (SAC) Index

Strain Age Cracking (SAC) was first introduced by Duvall and Owczarski, who linked it to HAZ cracking in nickel-based alloys during welding. They proposed that SAC occurs due to the interaction between residual stress relaxation and the aging precipitate phase (γ' phase). They developed a strain-ageing cracking susceptibility test to quantify the material's critical cracking conditions (e.g., critical strain threshold) by controlling factors such as temperature, strain rate, and aging time. This method laid the theoretical foundation for subsequent studies [75].

Yu et al. [87] studied the cracking behavior of nickel-based superalloys during additive manufacturing and introduced the SAC index. This index assesses the relationship between stress accumulation from precipitation and crack formation during alloy heat treatment, focusing on the impact of secondary phase precipitation (e.g., γ' phase) in the solid solution on the alloy's behavior. Specifically, the SAC is quantified by calculating the volume fraction of the γ' phase in the alloy and the effect of its temperature change on the

stress using the following equation:

$$SAC = \frac{dV_{\gamma'}}{dT} \tag{3}$$

Here, $V_{\gamma'}$ represents the volume fraction of γ', T denotes temperature, $\frac{dV_{\gamma'}}{dT}$ represents the rate of change in the volume fraction of γ' with temperature. Fig. 5 illustrates SAC sensitivity, comparing microstructural features corresponding to low and high strain-age crack sensitivity.

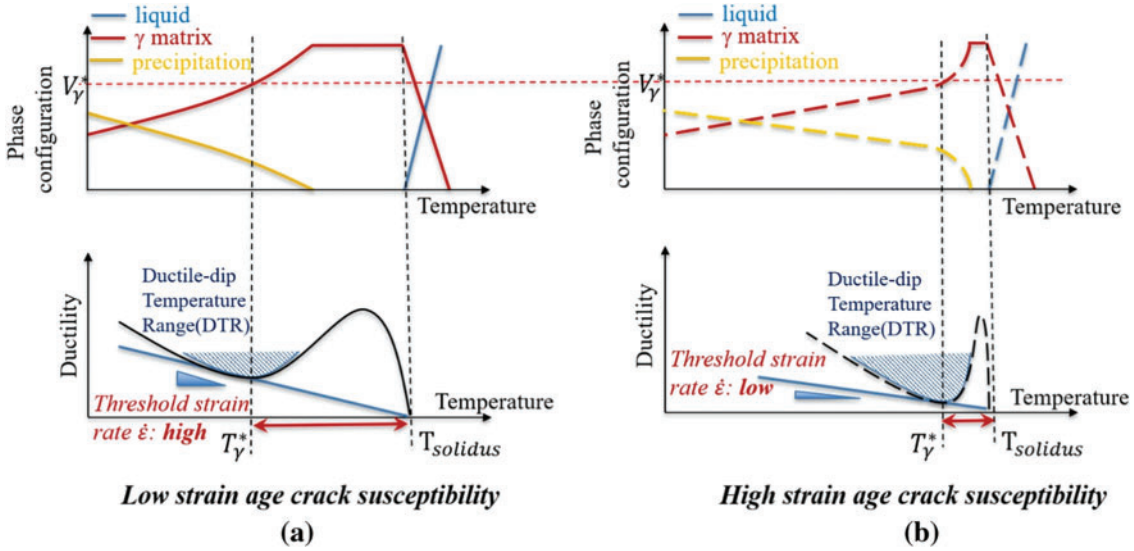

Figure 5: Schematic diagram of the susceptibility of strain-age cracks. (**a**) Schematic of low strain-age crack susceptibility with wide homogenization temperature range and gradual γ' precipitation. (**b**) Schematic of high strain-age crack susceptibility with narrow homogenization temperature range and abrupt γ' precipitation [87]

The SAC index, when combined with other related indices, has been applied to various research areas, including solidification cracking. For instance, Liu et al. [88] explored the reduction of crack susceptibility and enhancement of high-temperature performance in nickel-based superalloys during LPBF by optimizing the SCI, FR, and SAC indices. They designed a novel SD01 alloy and further enhanced its high-temperature mechanical properties by adding 1 wt.% TiB2 particles. This resulted in a significant improvement in tensile strength and elongation at 900°C compared to the pure SD01 alloy, attributed to the TiB2 particles modifying the morphology and increasing the volume fraction of the γ' phase.

3.5 Crack Sensitivity Coefficient (CSC)

Clyne and Davies [76] introduced the Crack Susceptibility Coefficient (CSC), which quantifies the time span of the mushy zone during the critical window of solidification based on the solid fraction in the semi-solid state. In the early stages of solidification, stress relaxation occurs through mass transport and liquid backfilling. In contrast, the later stages—characterized by a continuous but low-permeability liquid film—are more susceptible to thermal tearing due to restricted liquid replenishment. The CSC is defined as the ratio of the time interval during which the alloy is vulnerable to thermal cracking to the duration available for stress

relaxation, calculated as:

$$CSC = \frac{t_{f_s=0.99} - t_{f_s=0.90}}{t_{f_s=0.90} - t_{f_s=0.40}} \approx \frac{T_{f_s=0.99} - T_{f_s=0.90}}{T_{f_s=0.90} - T_{f_s=0.40}} \tag{4}$$

where f_s is the solid phase fraction in the semi-solid state and t is the time at a particular solid phase fraction. The numerator part corresponds to the time at which the solid phase fraction goes from 0.9 to 0.99, which is the stage prone to thermal tearing, and the denominator part corresponds to the time at which the solid phase fraction goes from 0.4 to 0.9, which is the stage of stress relaxation. Due to the extremely high cooling rate of the AM process, time and temperature can be approximated as linearly related, and thus the *CSC* can be approximated as a function of the temperature of the corresponding region. The coefficients have also been used to study the proposed optimised process parameters, which effectively reduce crack susceptibility and improve the quality of additive manufacturing of nickel-based superalloys [89].

3.6 Solid-State Cracking Criterion (M_{sac})

Strain age cracking (SAC) in nickel-based superalloys typically arises during thermal cycling or subsequent heat treatments. It results from the superposition of residual stresses and additional stresses induced by the precipitation of the γ' phase from the solid solution. To quantitatively evaluate SAC susceptibility, Thompson, later modified by Reed, proposed an empirical index based on the hypothesis that "the total content of γ'-forming elements (Al, Ti, Nb, and Ta) aggravates cracking by reducing local ductility." The central rationale is that a higher combined weight percentage of these γ'-forming elements enhances γ' precipitation, thereby intensifying the stresses generated during this process. When superimposed on residual stresses, this accumulation impairs the alloy's resistance to cracking [77,78]. This correlation is quantitatively described by the following equation:

$$M_{sac} = W_{Al} + 0.5W_{Ti} + 0.3W_{Nb} + 0.15W_{Ta} \tag{5}$$

The core principle of this index is to predict the susceptibility of alloys to strain age cracking (SAC) during hot working or in-service conditions based on the total concentration of critical γ'-forming elements. It provides a quantifiable foundation for evaluating cracking resistance during alloy design. This model has been widely adopted for assessing crack sensitivity in nickel-based superalloys, particularly in additive manufacturing, where SAC can be mitigated by compositional optimization of the key alloying elements.

3.7 SAC Risk Factor (RF)

According to Bartek Kaplan [79], the SAC risk index M_{sac}, derived from the total concentrations of Al, Ti, Nb, and Ta, is based on the overall alloy composition. While simple and convenient, this criterion cannot effectively distinguish between different cracking mechanisms and may misrepresent SAC susceptibility. Thermodynamically based approaches—although they account for variations in the γ'phase volume fraction with temperature and homogenization intervals—still suffer from several limitations. These include a lack of consideration for lattice mismatch effects and insufficient experimental validation. Kaplan concluded that alloy composition alone, such as that used in weldability diagrams, cannot be relied upon to differentiate among cracking mechanisms or to predict SAC susceptibility. In response to these limitations, Kaplan developed a more robust and widely applicable SAC risk factor by integrating key thermodynamic parameters that influence SAC behavior in nickel-based superalloys. The model is defined as follows:

$$R_{SAC} = -\frac{\nu^{\gamma'} \cdot \Delta}{T_{low}} \tag{6}$$

where $\Delta = \int_{T_{low}}^{T_{high}} \delta(T)\,dT$, $v^{\gamma'} = \int_{T_{low}}^{T_{high}} v_f^{\gamma'}(T)\,dT$, δ are the lattice mismatches and $v_f^{\gamma'}$ is the volume fraction of the γ' phase. However, the article also points out that the model can be used in the 2024a version of the Thermo-Calc performance module and can be easily applied to alloy design.

3.8 Thermal Resistance and Deformation Resistance (HR-DR) Modeling

Xu et al. [90] proposed a novel Heat Resistance-Deformation Resistance (HR-DR) model to address the cracking issues of nickel-based superalloys during the LPBF process. This model aims to predict the alloy's cracking susceptibility by analyzing the chemical compositional differences between the dendritic core (DC) and interdendritic (ID) regions during solidification. The study concluded that the alloy forms distinct DC and ID regions with differing chemical compositions during solidification, with these compositional variations being a primary contributor to cracking. The HR-DR model evaluates alloy printability—defined as the ability of an alloy to retain desirable properties during additive manufacturing processes—by calculating the thermal resistance (ΔT_S) and deformation resistance ($\Delta\sigma_y$) of both regions. The thermal resistance represents the ID region's resistance to heat during solidification relative to the DC region and is calculated as:

$$\Delta T_S = T_{S,ID} - T_{S,DC} \tag{7}$$

Here, $T_{S,ID}$ and $T_{S,DC}$ represent the solidus temperatures of the interdendritic (ID) and dendritic core (DC) regions are represented, respectively. These temperatures are determined using the solidus line gradients of individual alloying elements in the Ni-based superalloy, with the corresponding gradient values obtained from the Thermo-Calc® TCNI10 database. In contrast, the deformation resistance quantifies the difference in elastic load-bearing capacity between the ID and DC regions during mechanical deformation, and is defined as follows:

$$\Delta\sigma_y = \sigma_{y,ID} - \sigma_{y,DC} \tag{8}$$

Here, $\sigma_{y,ID}$ and $\sigma_{y,DC}$ denote the yield strengths of the interdendritic (ID) and dendritic core (DC) regions, respectively. The yield strength is calculated by incorporating multiple strengthening mechanisms, such as solid solution strengthening, grain boundary strengthening, and dislocation strengthening. The corresponding expression is given as follows:

$$\Delta\sigma_y = \sigma_p + \Delta\sigma_{SS} + \Delta\sigma_{GB} + \Delta\sigma_{\gamma'} + \Delta\sigma_{Dis} \tag{9}$$

In the proposed model, the difference in deformation resistance is evaluated by analyzing the compositional disparity between the interdendritic (ID) and dendrite core (DC) regions. Fig. 6 illustrates the distribution of chemical elements in both regions during solidification and demonstrates how this disparity is quantified using a simplified solute distribution approach. Specifically, Fig. 6a presents a schematic of the unit volume during solidification, where DC and ID refer to the dendrite core and interdendritic regions, respectively, with the Z-axis indicating the solidification direction. Fig. 6b,c depicts the solute concentration profiles and their simplified representations, which are used to calculate the compositional difference between the DC and ID regions.

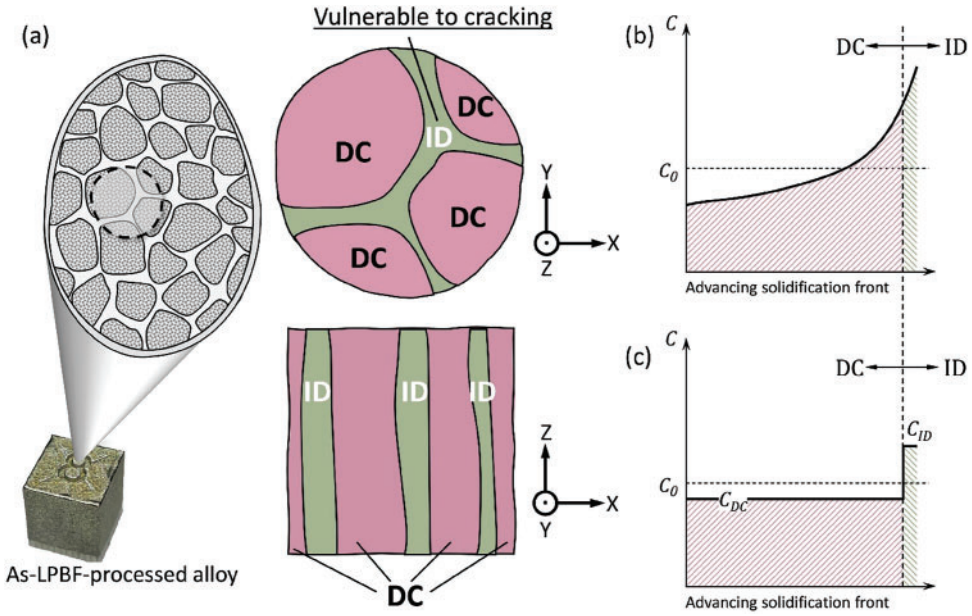

Figure 6: (**a**) Schematic illustration of a unit volume during solidification, the DC indicates the dendritic core region, while ID indicates the interdendritic region. Z is the direction of solidification. (**b**) Schematic illustration of the solute profile during solidification, and (**c**) schematic illustration of the simplified solute profile [90]

The HR-DR model establishes a direct correlation between alloy chemistry and cracking susceptibility during the LPBF process. This framework offers a theoretical foundation for optimizing both alloy composition and processing parameters to mitigate crack formation.

3.9 Thermal Shock Resistance (TSR)

Harrison [80] investigated the microcrack formation mechanisms in nickel-based superalloys during selective laser melting (SLM) and identified thermal shock-induced stress as the primary cause of cracking. Based on this observation, it was proposed that the "machinability" of an alloy—its ability to retain desirable properties during SLM—is closely linked to its Thermal Shock Resistance (TSR). A higher TSR correlates with reduced crack initiation and thus enhanced processability. The mathematical relationship can be described as follows:

$$TSR = \frac{\sigma_{UTS} \cdot \kappa \cdot (1 - \nu)}{E \cdot \alpha_{CTE}} \tag{10}$$

where σ_{UTS} represents the ultimate tensile strength of the material, κ is the thermal conductivity, ν is Poisson's ratio, E is Young's modulus, and α_{CTE} is the coefficient of thermal expansion. This model indicates that TSR is directly proportional to both tensile strength and thermal conductivity, while being inversely proportional to Young's modulus and the coefficient of thermal expansion. Based on the definition of TSR, Harrison et al. [91] proposed that increasing the tensile strength of alloys can enhance their TSR, thereby reducing the formation of microcracks during SLM processing. In their study on nickel-based superalloys, confirmed that higher tensile strength improves resistance to thermal shock-induced cracking, providing a theoretical basis for alloy optimization in SLM environments.

3.10 Tanaka-Mura's Model

In 1981, Tanaka and Mura [92] introduced a dislocation-based model, known as the Tanaka–Mura model, to describe fatigue crack initiation. This model analyzes the accumulation of dislocation dipoles by investigating slip band behavior in polycrystalline metals subjected to low-strain fatigue. It assumes that dislocations in two adjacent slip planes move in opposite directions and that their motion is irreversible. The model comprises three core mathematical expressions: the dislocation density equation, the stored strain energy equation, and the crack initiation life equation. The dislocation density equation characterizes the spatial distribution and accumulation of dislocations within slip bands under cyclic loading conditions. It is mathematically expressed as follows:

$$D_k(x) = (-1)^{k+1} \frac{(\Delta\tau - 2k)\, x}{\pi A \left(a^2 - x^2\right)^{1/2}} \tag{11}$$

where $D_k(x)$ represents the dislocation density at the kth step, $\Delta\tau$ is the stress range, k is the number of cycles, Δ is a material-dependent constant, and a is the length of the dislocation stack.

The stored strain energy formula, on the other hand, calculates the energy stored by the accumulation of dislocations and is expressed as:

$$U_k = (-1)^{k+1} \frac{1}{2} \int \tau_1^D \phi(x)\, dx \tag{12}$$

Here, U_k denotes the stored strain energy at the kth step, τ_1^D is the back stress due to dislocation, ϕ(x) is the plastic displacement due to dislocation motion, and k is the number of cycles. The accumulation of stored strain energy is an important indicator of fatigue crack initiation.

The crack initiation life equation is based on the relationship between the stored strain energy and the fracture energy of the material, and the crack initiates when the stored strain energy reaches a certain threshold, which is expressed as:

$$n_c = \frac{4\omega_s}{(\Delta\tau - 2k)\,\Delta\gamma} \tag{13}$$

where n_c is the lifetime of crack initiation, ω_s is the fracture energy of the material, $\Delta\tau$ is the stress range, k is the frictional stress, and Δ and γ are material and geometry-related constants.

Together, these equations form the mathematical basis of the Tanaka-Mura model for describing and predicting fatigue crack initiation and early extension behaviour in polycrystalline metals. The model also successfully explains the relationship between fatigue crack emergence life and plastic strain range in accordance with the Coffin-Manson law, and the relationship between fatigue strength and grain size in accordance with a Petch-type equation.

Building upon the Tanaka-Mura model, Liu and Lu [93] proposed an improved Tanaka-Mura model to more accurately predict the microcrack initiation life of metallic materials, focusing on nickel-based superalloys as an example. The improved model introduces the slip irreversibility parameter (SIP) and incorporates slip hardening behavior, addressing the limitations of the original model in terms of slip irreversibility assumptions and critical resolved shear stress (CRSS) treatment. This allows the model to more realistically reflect the influence of material microstructure on the fatigue damage process. Numerical simulations were conducted to verify the accuracy of the improved model, and comparisons with experimental results were performed. The findings demonstrate that the improved model can more accurately predict the microcrack

initiation life of nickel-based superalloys and reveal the effects of slip irreversibility and slip hardening on fatigue life.

The combination of microscopic dislocation motion with macroscopic fatigue properties through the Tanaka-Mura model provides insights into understanding the fatigue behaviour of materials. For example, Cui et al. [94] utilized the cyclic slip dislocation stacking model from the Tanaka-Mura theory. By substituting the material's mechanical property parameters into the equations and combining them with the finite element method (FEM) to simulate the crack initiation process in polycrystalline metallic materials, they successfully predicted the low-cycle fatigue life of Inconel 718 alloy under varying surface integrity conditions.

3.11 Generalised Hot Cracking Criterion

Chandra et al. [81] systematically investigated hot cracking mechanisms in nickel-based single-crystal superalloys fabricated via selective electron beam melting (SEBM), a metal additive manufacturing technology. Through multi-scale experimental characterization and numerical simulations, they elucidated the critical role of divergent grain boundaries and solidification parameters (e.g., cooling rate, thermal gradient) in crack initiation. A generalized hot cracking criterion was proposed by modifying Kou's model to incorporate grain boundary inclination angles, enabling quantitative prediction of crack susceptibility. In nickel-based superalloys manufactured by SEBM, severe thermal cracking is susceptible to occur at grain boundaries (GBs), especially at divergent grain boundaries. It has been found that microdeviation occurs at all grain boundaries, but it is more pronounced at evanescent grain boundaries, promoting crack formation. In order to gain a deeper understanding of this phenomenon, the authors used multiscale numerical simulations to determine solidification parameters and grain growth, revealing the impact of different grain boundary types on thermal cracking.

In their study, special attention was paid to the effect of grain boundary tilt angle (θ) on thermal cracking behaviour. Fig. 7 schematically illustrates the growth of two tilted grains during solidification and highlights the characteristics of grain boundaries at different tilt angles. Fig. 7a shows the tilt angle θ of two neighbouring grains in the growth direction, Fig. 7b shows the cross-section of the grains at a specific height z, Fig. 7c illustrates the final geometry of the grains at the later stage of solidification, and Fig. 7d depicts the region of the liquid-phase channel at the grain boundaries, where the liquid is transported at a velocity v_z. These schematics help to understand how the angle of inclination of the grain boundary affects the flow and feeding of the liquid phase, which in turn affects the formation of thermal cracks.

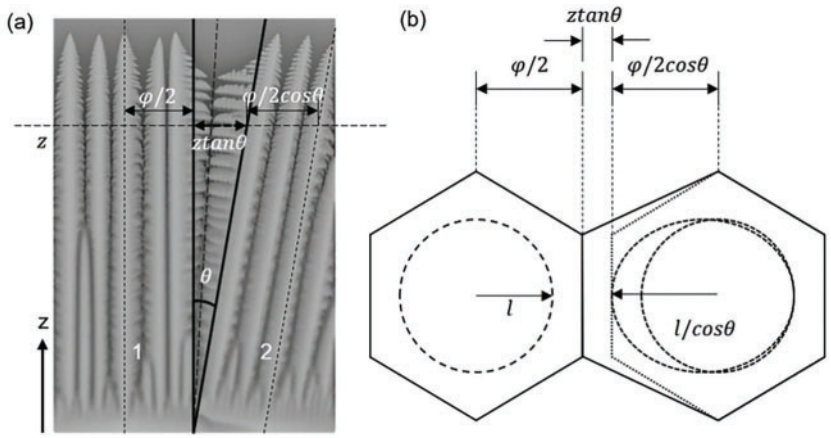

Figure 7: (Continued)

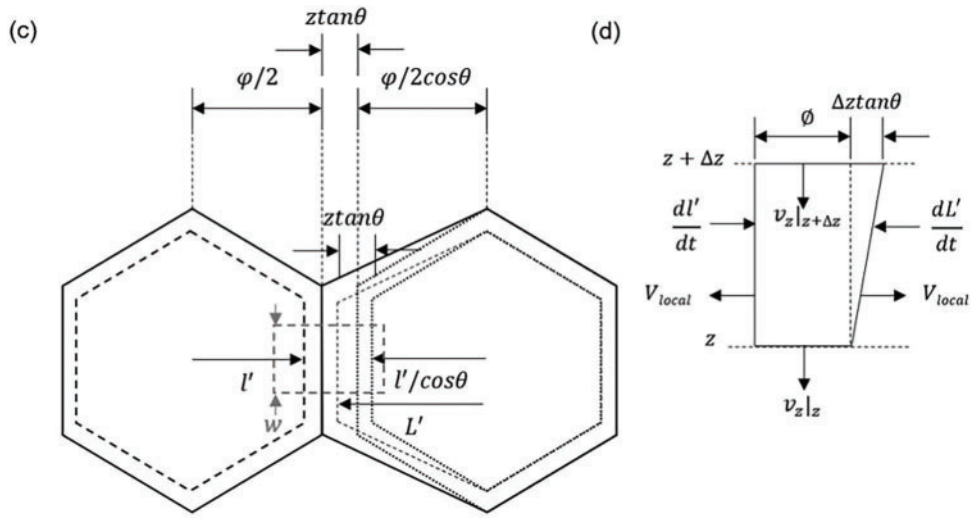

Figure 7: Schematic of grain growth during solidification. (**a**) In a 2D plane along the build direction, (**b**) cross-section in XY-plane at a particular height z. (**c**) Grain cross-section at the terminal stage of solidification and (**d**) liquid channel at the grain boundary during solidification [81]

Based on the existing thermal cracking criterion, Chandra et al. extended and improved it to propose a generalised thermal cracking criterion. This criterion not only considers a variety of process parameters, but also specifically introduces the critical factor of grain boundary tilt to more accurately predict and explain the thermal cracking behaviour of nickel-based superalloys during the additive manufacturing process. The mathematical expression of the guideline is given below:

$$\frac{d\varepsilon_{local}}{dt} > \left[\frac{\sqrt{1-\beta}}{2}\cdot\left|\frac{d\sqrt{f_s}}{dT}\right|\cdot\left(1+\frac{1}{cos\theta}\right)\cdot|CR| - \frac{tan\theta}{\varphi}\cdot\frac{|CR|}{G}\right] + \frac{d}{dz}\left[\frac{1}{2}\left(1-\sqrt{1-\beta}\cdot\sqrt{f_s}\right)\cdot\left(1+\frac{1}{cos\theta}\right)\cdot v_z\right]_z \tag{14}$$

where $\frac{d\varepsilon_{local}}{dt}$ is the local segregation term, which represents the crack extension due to solidification shrinkage and thermal shrinkage; β is the shrinkage rate, the ratio of the difference between the solid and liquid densities to the liquid density; $\frac{d\sqrt{f_s}}{dT}$ is the rate of change of the square root of the solid fraction with respect to the temperature; CR is the cooling rate; θ is the angle of tilt of the grain boundaries; ϕ is the grain width; G is the temperature gradient; v_z is the liquid feeding rate along the growth direction; and f_s is the solid phase fraction. The proposal of this generalised thermal cracking criterion provides an important theoretical basis for the prevention and control of thermal cracking during the additive manufacturing of nickel-based superalloys.

4 Component Design Strategy

4.1 Functional Modulation of Key Alloying Elements

4.1.1 Strengthening Elements (Al, Ti)

Aluminum (Al) and titanium (Ti), the primary strengthening elements in nickel-based superalloys, significantly enhance high-temperature strength and creep resistance by promoting the precipitation of

the γ' phase (Ni_3(Al, Ti)) [95]. Moreover, they inhibit crack formation by refining the grain structure and optimizing the microstructural characteristics [96]. First, Al and Ti additions promote grain refinement and microstructural optimization. Fine grains reduce local stress concentrations, thereby lowering the likelihood of crack initiation. In additive manufacturing, fine-grained structures help mitigate thermal cracking by enhancing stress distribution and minimizing localized stress buildup [97]. Second, Al and Ti improve creep resistance by promoting γ' phase precipitation. At elevated temperatures, this phase impedes dislocation slip and climb, thereby enhancing creep resistance. This mechanism also contributes to crack growth suppression while maintaining elevated-temperature strength. For instance, increasing Al and Ti concentrations has been shown to enhance creep resistance and reduce crack formation [98].

Additionally, Al and Ti enhance the oxidation resistance and thermal stability of the alloy. Under high-temperature conditions, these elements form a dense oxide layer that shields the alloy from oxidative degradation. This protective effect reduces oxidation-induced cracking and enhances alloy reliability [99]. However, excessive Al and Ti contents may increase the alloy's susceptibility to cracking by promoting the formation of the γ–γ' eutectic phase. This phase can weaken grain boundaries by creating localized compositional inhomogeneities, thereby facilitating both solidification and liquation cracking. Therefore, precise control of Al and Ti content is essential. Optimizing these elemental contents can effectively suppress crack initiation and improve the overall performance of the alloy [98]. Fig. 8 illustrates the influence of Al and Ti content on the weldability of nickel-based superalloys. As shown, alloys with combined Al + Ti content exceeding 4.5 wt% are considered "unweldable".

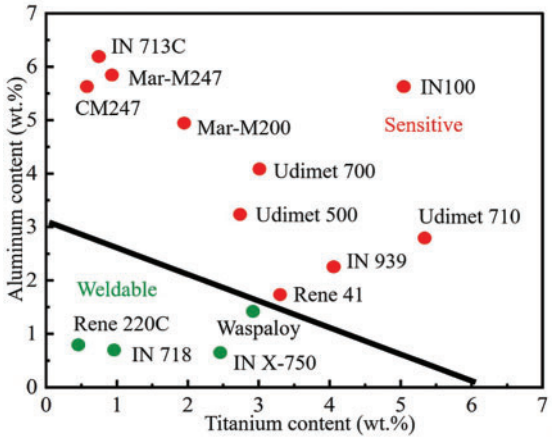

Figure 8: Weldability diagram based on Ti and Al content [100]

4.1.2 Grain Boundary Strengthening Elements (B, Zr, Re)

In nickel-based superalloys, grain boundary-strengthening elements such as boron (B), zirconium (Zr), and rhenium (Re) play a critical role in enhancing high-temperature performance. They improve grain boundary stability through distinct mechanisms, thereby increasing both crack resistance and structural integrity under elevated-temperature conditions.

In nickel-based superalloys, B primarily enhances grain boundary properties by forming stable borides during precipitation. These borides possess high melting points and exhibit excellent corrosion and oxidation resistance, effectively mitigating grain boundary embrittlement and suppressing crack initiation and propagation [101–104]. Yu et al. [34] investigated the role of boron in nickel-based superalloys, revealing that boron primarily enhances intergranular stability through the formation of stable borides at grain

boundaries. These borides contribute to reduced embrittlement and enhanced resistance to crack initiation and growth. By introducing γ/MC phase boundaries to regulate boron distribution, the newly developed Additive Manufacturable Superalloys with no Distribution of boron (AMSC-DB) alloys demonstrated excellent printability and mechanical performance in additive manufacturing, validating the effectiveness of this compositional strategy.

Zr, another key grain boundary-strengthening element, significantly enhances grain boundary stability in nickel-based superalloys. Its addition improves crack resistance by forming stable compounds or solid solutions through interactions with other alloying elements, thereby reinforcing the grain boundary region [105,106]. Zr polarization at grain boundaries enhances their toughness, which inhibits crack propagation caused by stress concentration or thermal fatigue. Zhou et al. [107] examined the polarization behavior of Zr in the IN100 nickel-based superalloy and its impact on microstructural evolution. They reported that Zr segregated at the eutectic/matrix interface, forming $Ni_{11}Zr_9$ intermetallics. Zr addition also lowered the alloy's solidus temperature, altered the solidification range, promoted γ–γ' eutectic formation, and influenced carbide morphology. The polarization effect contributed to improved grain boundary toughness, suppressing crack growth from thermal or mechanical stress. Additionally, Zr improves oxidation resistance, thereby enhancing the alloy's overall high-temperature performance [108,109]. However, Zr may also promote cracking under certain conditions. Zhang et al. [110] investigated the influence of Zr and boron (B) on hot tearing susceptibility in IN792 superalloys during directional solidification (DS). They found that Zr or B alone had limited influence on casting behavior. However, the simultaneous presence of Zr and B significantly increased hot tearing tendency, particularly at high Zr concentrations. This synergistic effect likely promotes the formation of continuous liquid films at grain boundaries during the terminal stage of solidification, weakening intergranular cohesion and increasing hot tearing risk.

Re is a critical strengthening element in nickel-based superalloys, particularly effective in enhancing high-temperature stability, creep resistance, and fatigue life [111–113]. Zhao et al. [114] studied the creep behavior of single-crystal superalloys containing 4.5% Re and 3.0% Ru under 1040°C–1070°C and 137–180 MPa loading conditions. The alloy exhibited excellent creep resistance, with dominant mechanisms including dislocation climb and shearing into the rafted γ' phase. Formation of Kear-Wilsdorf (K-W) locks was observed, which hindered dislocation slip and cross-slip, thereby improving creep resistance. Crack initiation and propagation occurred along the γ/γ' interface, ultimately resulting in creep rupture. Re addition enhances dislocation network stability, inhibits dislocation mobility, and significantly improves high-temperature strength and creep resistance [115]. Re also contributes to improved fatigue resistance by stabilizing the dislocation structure and delaying crack initiation, thereby extending fatigue life. Ding et al. [116] observed that Re atoms segregate at tensile regions near interfacial dislocation cores, forming a Cottrell atmosphere. *In situ* Transmission Electron Microscope (TEM) and SEM analyses confirmed that the Re-enriched dislocation network suppresses dislocation motion and crack propagation, thereby enhancing creep performance.

4.1.3 Control of Impurity Elements (C, O)

In the compositional design of additively manufactured nickel-based superalloys, precise control of impurity elements, particularly carbon (C) and oxygen (O), is essential for suppressing liquation cracking and enhancing high-temperature performance. Impurity elements typically form low-melting-point eutectic or precipitate phases in alloys, which are particularly prone to liquation cracking at elevated temperatures. These phases, often concentrated at the grain boundaries, cause localized melting and embrittlement, accelerating crack initiation and propagation.

O is a common impurity in nickel-based superalloys. It readily forms oxide inclusions that degrade mechanical performance and often act as initiation sites for cracking. Ryou et al. [117] examined thermal cracking in IN738 superalloy fabricated via direct laser deposition (DLD), attributing the cracks to Ni and Mo oxide particles precipitated within grains and along grain boundaries. Atom probe tomography (APT) revealed a transitional zone between the oxide particles and the surrounding matrix, where oxygen is dissolved in solid solution. This alters local chemistry and reduces the matrix melting point. Upon reheating during DLD, these oxide inclusions facilitate stress concentration and initiate liquation cracking. Qiu et al. [118] observed that Al-, Si-, and W-rich oxide particles with high melting points preferentially nucleate during solidification, preceding the growth of γ-cellular structures. These oxides, along with fine grains, promoted crack formation, typically at γ grain–oxide interfaces or along the midline of oxide clusters. This behavior is primarily driven by solidification shrinkage and thermal contraction. Furthermore, segregation of Si, W, and O at specific grain boundaries causes embrittlement, further accelerating crack propagation.

Carbides represent another key factor contributing to crack formation. For instance, Xu et al. [119] examined crack initiation in the overlapping zone (OZ) of IN738LC alloy processed via Laser Solid Forming (LSF). They reported that carbide accumulation at grain boundaries induces local stress concentration and obstructs liquid-phase flow, both of which promote crack formation, as illustrated schematically. Carbide-enriched grain boundaries act as crack initiation sites, with cracks propagating preferentially along high-angle grain boundaries during subsequent deposition. The precipitation of carbides is closely linked to elemental microsegregation. Elements such as Ti, Nb, Ta, and Mo tend to segregate at grain boundaries, where they facilitate carbide formation. Moreover, carbides reduce the wettability and mobility of the liquid phase, impairing its ability to fill grain boundary voids during solidification. This deficiency promotes crack extension (Fig. 9).

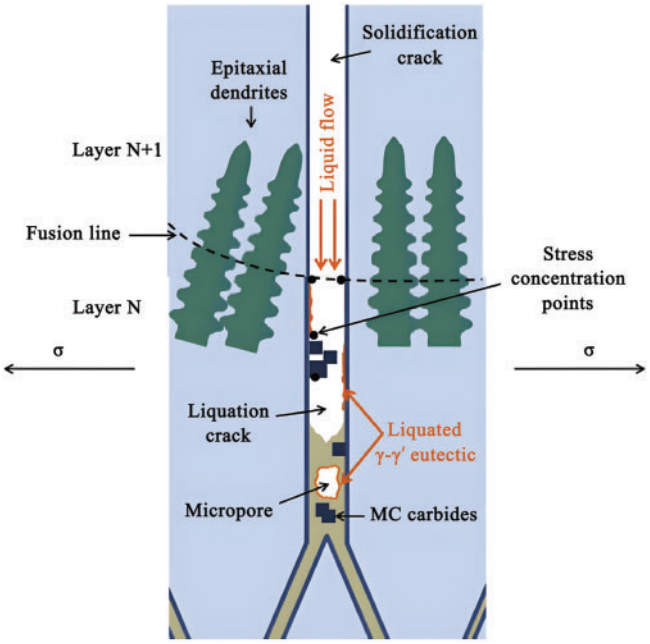

Figure 9: Schematic diagram of liquefaction and solidification crack initiation facilitated by carbides at grain boundaries impeding liquid phase flow at grain boundaries [119]

Messé et al. [120] performed a detailed analysis of the microstructural evolution in SLM-processed IN738LC superalloy subjected to various heat treatment conditions. Their results revealed that carbides influence crack formation by altering both the microstructure and stress distribution. Specifically, a uniform distribution of fine MC carbides along grain and cell boundaries mitigates stress concentration, thereby reducing crack initiation. However, during stress relief heat treatment, the transformation of metastable MC carbides into more stable $M_{23}C_6$ carbides alters their size and distribution, potentially causing local stress redistribution and elevating crack formation. Moreover, carbide transformation and coarsening can detrimentally impact the alloy's plasticity and toughness, thereby affecting subsequent crack propagation.

To inhibit liquation cracking, it is essential to minimize oxide and carbide formation by controlling impurity levels, particularly O and C, in the superalloy. This objective can be attained by employing high-purity raw materials, optimizing the alloy composition, and implementing refining and de-impurity processes.

4.2 Application of Efficient Component Design Methods

4.2.1 Thermodynamically Assisted Compositional Design

Thermodynamically assisted composition design is an alloy design approach that leverages thermodynamic principles and computational tools to optimize alloy compositions by predicting phase behavior and thermophysical properties. In designing nickel-based superalloys, this approach plays a critical role. By combining thermodynamic calculations with machine learning, researchers can tailor alloy compositions to meet targeted performance criteria. For example, thermodynamic parameters of nickel-based powder superalloys, including initial melting temperature (T_m), complete dissolution temperature of γ' phase ($T_{\gamma'}$), γ' phase content, γ/γ' lattice mismatch ($|d|$), and topologically close-packed phases (TCPs) content, have been calculated using JMatPro software. These calculations offer a vital theoretical foundation for alloy composition optimization [121]. Studies have demonstrated that adjusting alloy compositions markedly influences thermodynamic properties; for example, increasing the contents of Co, Cr, Mo, and W raises T_m, thereby enhancing high-temperature performance. Moreover, regulating the levels of Al, Ti, Ta, and Nb allows control over γ' phase fraction and lattice mismatch, thereby optimizing the alloy's strengthening effect [121]. Furthermore, managing TCP content is essential to mitigate alloy brittleness. The workflow for alloy composition design in this study is illustrated in Fig. 10.

Further studies optimized the composition of the IN738 superalloy using thermodynamic calculations. A novel alloy, designated IN738M, was developed by adjusting the contents of Co, C, and Hf, which effectively suppressed crack formation. The optimized alloy exhibited excellent machinability during laser powder bed fusion (LPBF) and enabled crack-free fabrication, even at a high γ' phase mass fraction [122]. These findings suggest that thermodynamically assisted compositional design can markedly enhance the machinability and mechanical performance of superalloys, effectively mitigating cracking, a challenge that conventional manufacturing methods struggle to overcome.

Additionally, a multi-physics modeling framework integrating thermodynamic calculations and evaporation models was employed to investigate compositional changes in nickel-based superalloys during laser powder bed melting. By controlling process parameters—such as laser power, scanning speed, and powder layer thickness—the evaporation loss of alloying elements can be effectively minimized, thereby optimizing the alloy's composition and properties [123]. This work provides a robust theoretical foundation for the compositional control of nickel-based superalloys in additive manufacturing.

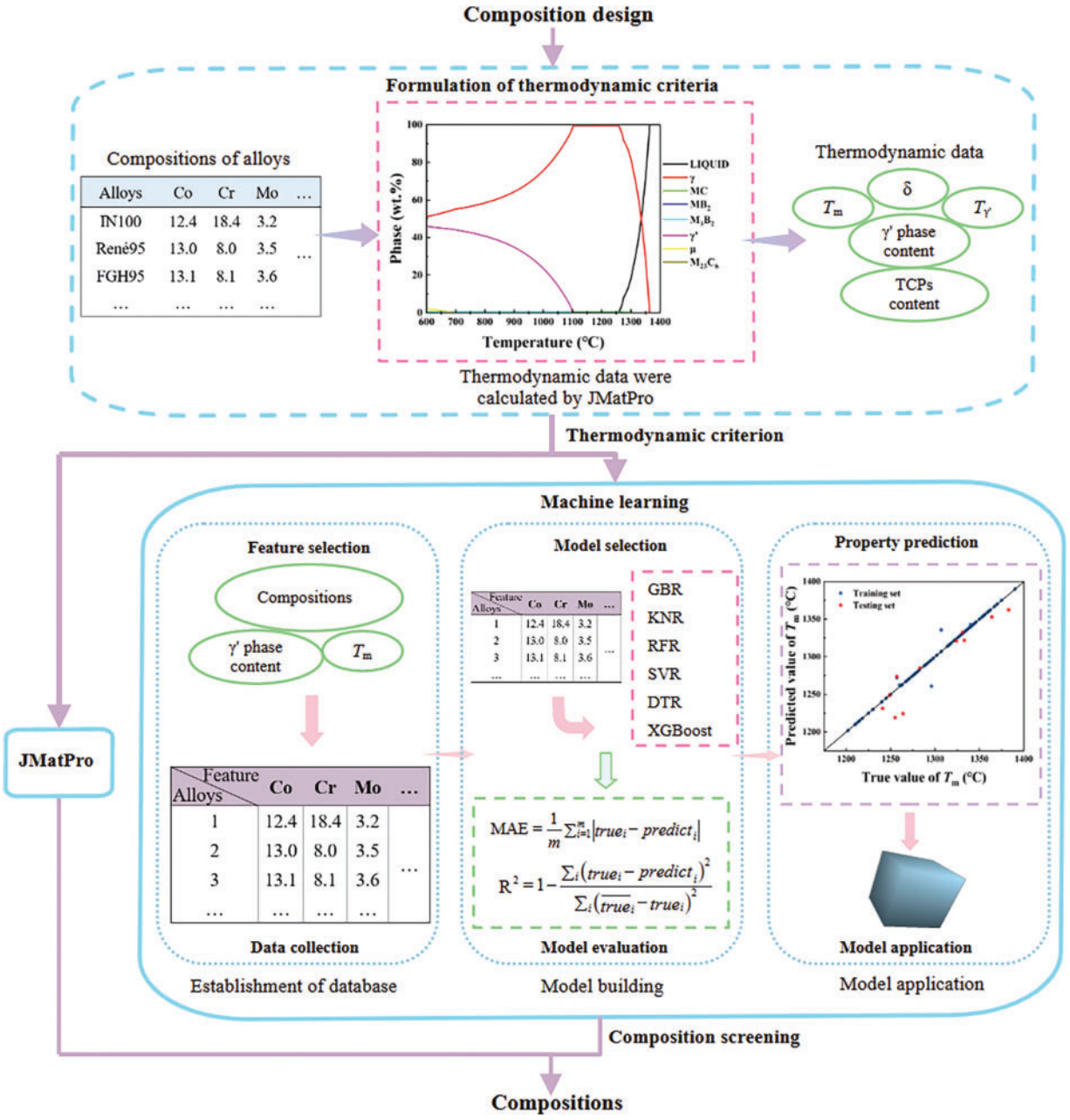

Figure 10: The workflow of alloys composition design [121]

4.2.2 High-Throughput Experiments to Aid in Component Design

High-throughput experiment-assisted compositional design is a method that rapidly synthesizes and tests numerous alloy samples with varying compositions using automated experimental techniques and efficient data acquisition, thereby accelerating materials research and development [124,125]. In the development of nickel-based superalloys, this approach not only enhances experimental efficiency but also establishes a data-driven paradigm for composition optimization. By systematically acquiring multidimensional material property data, it lays a robust foundation for constructing a composition–structure–property correlation model [126].

Notably, this data-driven approach is spurring innovative research methods. A prime example is the semi-supervised deep transfer learning framework developed by Yang's team. By leveraging extensive microscopic image data from high-throughput experiments, they combined the UNet++ (A Nested U-Net Architecture for Medical Image Segmentation) network with adversarial training to accurately identify the γ' phase under various heat treatment conditions This breakthrough demonstrates that standardized big data from high-throughput technologies can significantly enhance the generalization of machine learning models, even in small sample scenarios—thus opening new avenues for engineering applications in microstructure recognition [127].

High-throughput technology's value extends beyond experimental efficiency; its integration with computational methods broadens research dimensions. For example, Wang's team demonstrated this synergistic effect. They evaluated the solid solution strengthening of 35 binary alloys using a high-throughput density functional theory (DFT) computational system combined with the Labusch model to elucidate the strengthening mechanism arising from lattice and modulus mismatch. This "computation-first, experimental-validation" paradigm transforms high-throughput technology from a simple experimental accelerator into a theory-guided compositional screening tool, significantly enhancing the scientific predictability of alloy design [128].

In addition, frontier exploration in this field is advancing toward full-process integration. For example, Ouyang's team has developed a novel superalloy, IN738M, with performance surpassing Haynes 282 by targeting potential compositional space via high-throughput DFT calculations and promptly proceeding to experimental validation. This closed-loop paradigm—integrating computation and experimentation—demonstrates that fine-tuned composition regulates mechanical properties and oxidation resistance, while underscoring the pivotal role of high-throughput technology in a multi-scale R&D framework. It not only predicts material behavior at the atomic level but also rapidly validates design assumptions at the macro scale, thereby shifting materials development from empirical trial-and-error to rational design [129]. Vecchio et al. [130] investigated the High-Throughput Rapid Experimental Alloy Development (HT-READ) methodology, as illustrated in Fig. 11. The figure delineates the entire HT-READ workflow, spanning computational screening, sample library synthesis, processing, characterization, testing, and subsequent analysis. Specifically, candidate materials are computationally screened using CALculation of PHAse Diagrams (CALPHAD) and machine learning models, followed by sample library synthesis via 3D printing and automated high-throughput processing, characterization, and testing. The newly generated data then informs iterative design improvements, creating a closed-loop materials development process. This workflow markedly enhances the efficiency and speed of materials development.

4.2.3 Machine Learning Assisted Component Design

Nowadays, machine learning—a data-driven tool—has been effectively employed for predicting material performance and exploring new materials, demonstrating exceptional efficiency and accuracy. Given its unique capability to decipher complex relationships between material descriptors and properties, machine learning has emerged as a promising approach for property prediction in Ni-based superalloys [131–134]. Simultaneously, data-driven methods can enhance the intelligence of additive manufacturing, thereby addressing critical challenges. In this context, machine learning is pivotal; by analyzing vast amounts of high-dimensional data, it rapidly identifies patterns and predicts outcomes, thereby optimizing process parameters, manufacturing efficiency, and product quality. Fig. 12 below presents a conceptual diagram of this model.

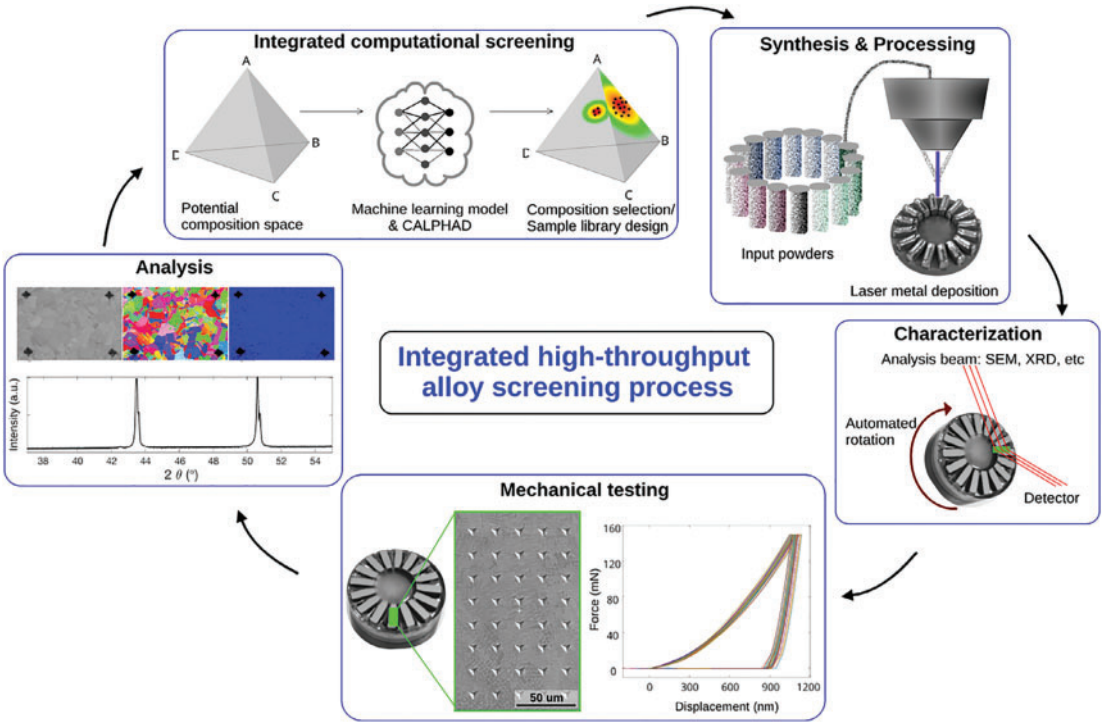

Figure 11: Illustration of the steps incorporated into the integrated High-Throughput Rapid Experimental Alloy Development (HT-READ) methodology [130]

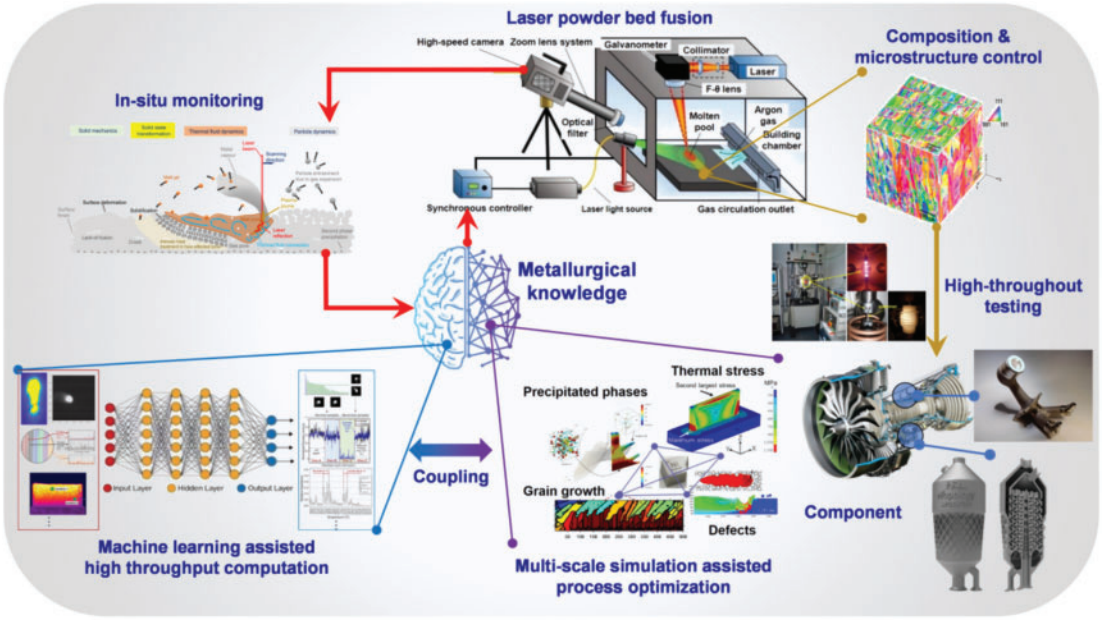

Figure 12: Conceptual illustration of "Ready-to-use" model for manufacturing Ni-based superalloys through laser powder bed fusion [135]

In nickel-based superalloy design, machine learning algorithms accelerate alloy development by inferring new formulations and predicting properties from existing composition-property data. Tan et al. [136] used a machine learning approach based on support vector regression (SVR) to model uniform fatigue life and estimate uncertainty for various nickel-based alloys, including polycrystalline, columnar, and single-crystal alloys. The SVR model was constructed using 1317 sets of fatigue data, incorporating material- and loading-related input variables. A non-Bayesian model fusion approach estimated the model's uncertainty and data dependence. The SVR model outperforms classical fatigue life models in predicting the lifespan of nickel-based alloys across various loading conditions and fatigue regimes. The best model accuracy and stability were achieved when 70% of the data were used for training. Pearson's correlation analysis and key feature reorganization revealed that total strain range and test frequency strongly correlate with fatigue life. The downscaled SVR model maintained acceptable accuracy, offering a useful tool for fatigue studies under complex loading conditions.

Scholars have integrated machine learning with multi-objective optimization algorithms to optimize the composition of nickel-based superalloys [137]. Using thermodynamic simulation data, Pearson correlation analysis determined microstructural parameters related to high-temperature tensile strength and elongation. A machine learning model was then developed and used to perform a global search in high-dimensional compositional space with a multi-objective evolutionary algorithm to identify candidate alloy compositions that meet design specifications. The microstructures and properties of these candidate alloys were experimentally verified, leading to the successful design of a nickel-based superalloy that met the target requirements and constraints. The intelligent design process is illustrated in Fig. 13.

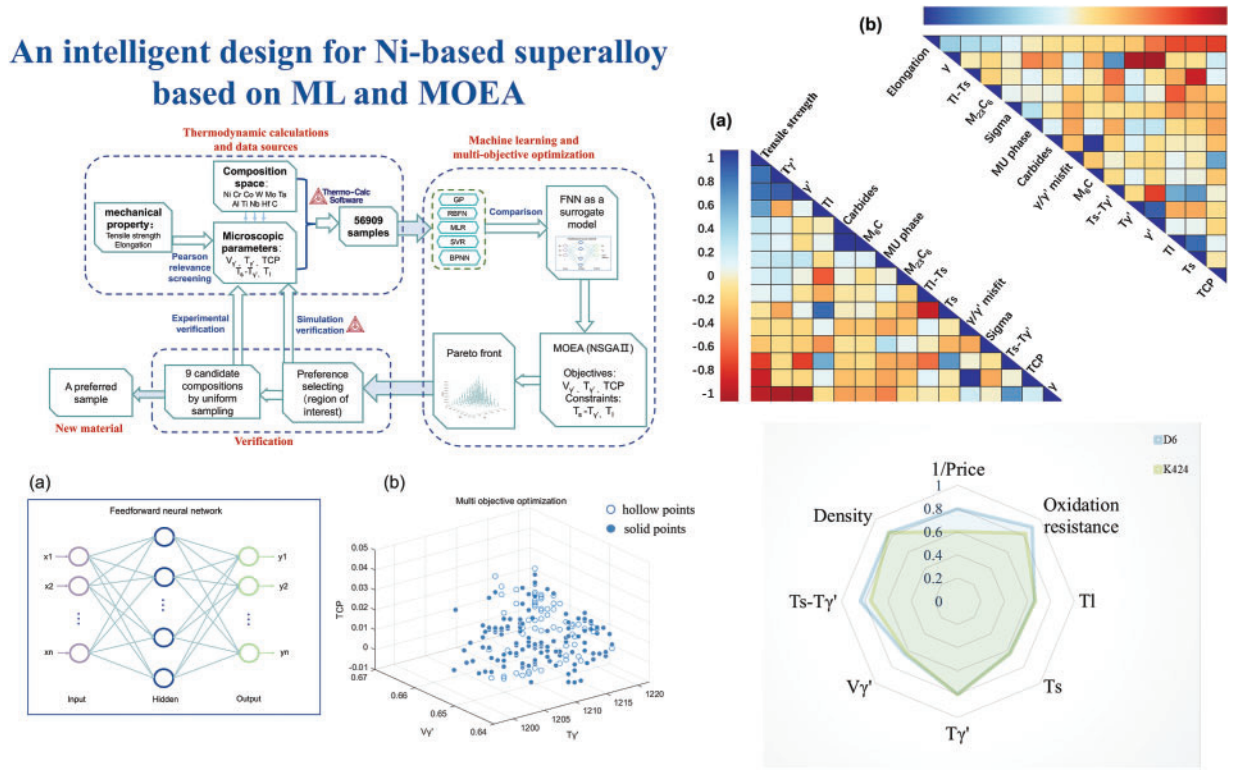

Figure 13: Intelligent design process and results of nickel-based high-temperature alloy based on machine learning and multi-objective optimization [137]

The application of machine learning in alloy design primarily depends on a substantial amount of experimental data. This data typically includes the alloy's composition ratio and corresponding property metrics, such as high-temperature strength, creep resistance, fatigue resistance, and oxidation resistance [138]. By collecting and organizing this data, researchers can train machine learning models to understand the complex, nonlinear relationship between alloy composition and its properties. For instance, Gao et al. [139] explored the use of machine learning to aid in designing nickel-based superalloys with superior high-temperature properties. Fig. 14 illustrates the design strategy used in this study, which includes collecting datasets, training an artificial neural network to predict mechanical properties at high temperatures, and screening new alloy compositions with optimized properties.

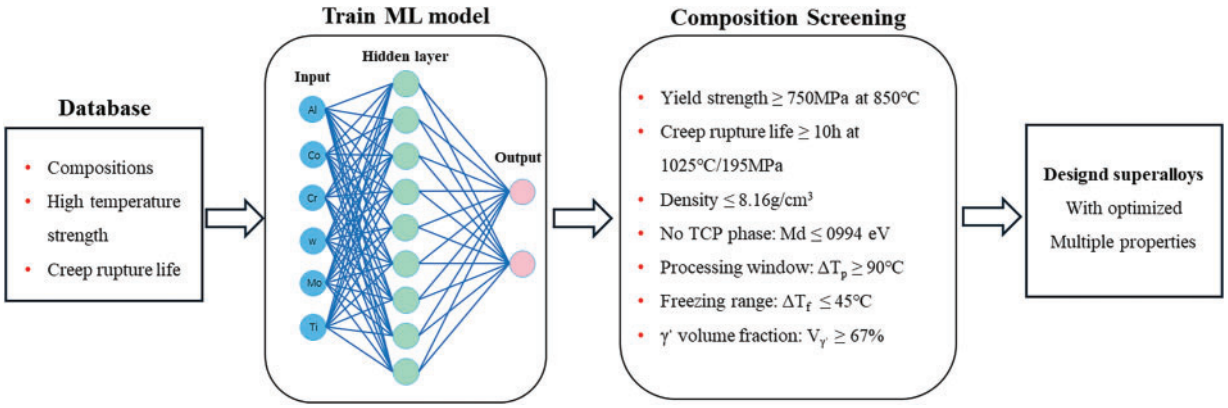

Figure 14: Superalloy design strategy [139]

In designing nickel-based superalloys, machine learning enables the evaluation of how various reinforcing elements influence the alloy's high-temperature properties [140]. Through model training, researchers can identify specific elemental ratios and concentrations that significantly enhance performance, thereby guiding the compositional optimization process.

However, the predictive accuracy of machine learning models is highly dependent on both the quality and volume of experimental data. Insufficient datasets or significant experimental errors can result in unreliable or biased model predictions. Thus, ensuring high-quality and diverse experimental datasets is essential for the robust and reliable application of machine learning in superalloy design.

5 Conclusion

This review integrates computational modeling with experimental insights to address cracking challenges in additively manufactured nickel-based superalloys. Through the analysis of multiple crack sensitivity models—including the Rappaz-Drezet-Gremaud (RDG) criterion, solidification cracking index (SCI), thermal shock resistance (TSR), and generalized hot cracking criterion—we establish a comprehensive framework for predicting and mitigating defects in AM components. These models provide critical insights into the interplay between alloy composition, processing parameters, and crack formation mechanisms, enabling targeted strategies to enhance the reliability and performance of additively manufactured superalloys.

However, significant challenges remain in fully capturing the complexity of crack behavior under multi-physics conditions. Current models often simplify the effects of microstructural heterogeneity and non-linear thermal-mechanical interactions, limiting their predictive accuracy in real-world applications. Future

research should focus on developing hybrid modeling approaches that integrate machine learning with traditional physics-based models to better capture these complexities. Additionally, real-time simulation of thermal-mechanical loads during AM processes could further refine predictive capabilities. The integration of *in-situ* experimental data with computational frameworks also holds promise for validating and improving model robustness. Overall, advancements in modeling methodologies will be crucial for accelerating the development of next-generation nickel-based superalloys tailored for additive manufacturing.

Acknowledgement: The authors would like to express their gratitude for the support received from the Aero Engine Corporation of China, the Young Elite Scientists Sponsorship Program by CAST, the High Performance Computing Center of Central South University, and the State Key Laboratory of Powder Metallurgy, Central South University, Changsha, China. This work was made possible through their generous contributions and resources.

Funding Statement: This study was supported by the Aero Engine Corporation of China [Grant No. HFZL2022CXY029], the Young Elite Scientists Sponsorship Program by CAST [2022QNRC001], the High Performance Computing Center of Central South University, and the Project Supported by State Key Laboratory of Powder Metallurgy, Central South University, Changsha, China.

Author Contributions: The authors confirm their contribution to the paper as follows: Huabo Wu and Jialiao Zhou contributed to writing—original draft and literature research; Lan Huang and Feng Liu contributed to conceptualization, supervision, and project administration; Zi Wang and Liming Tan contributed to writing—review & editing; Jin Lv contributed to literature collection and research. All authors reviewed the results and approved the final version of the manuscript.

Availability of Data and Materials: All data generated or analyzed during this study are included in this published article.

Ethics Approval: Not applicable.

Conflicts of Interest: The authors declare no conflicts of interest to report regarding the present study.

References

1. Gudivada G, Pandey AK. Recent developments in nickel-based superalloys for gas turbine applications: review. J Alloys Compd. 2023;963:171128. doi:10.1016/j.jallcom.2023.171128.
2. Sreenu B, Sarkar R, Kumar SSS, Chatterjee S, Rao GA. Microstructure and mechanical behaviour of an advanced powder metallurgy nickel base superalloy processed through hot isostatic pressing route for aerospace applications. Mater Sci Eng A. 2020;797:140254. doi:10.1016/j.msea.2020.140254.
3. Kumar D, Idapalapati S, Wei W. Microstructural response and strain hardening in deep cold rolled nickel-based superalloy for aerospace application. Procedia CIRP. 2018;71(12):374–9. doi:10.1016/j.procir.2018.05.044.
4. Li JG, Wang N, Liu JD, Xu W. Influence of rare earth elements (Y, La and Ce) on the mechanical properties and oxidation resistance of nickel-based superalloys: a critical review. J Mater Sci Technol. 2024;195(139):9–21. doi:10.1016/j.jmst.2023.11.077.
5. Xi X, Lin D, He Z, Ma R, Wei H, Shi Z, et al. Additively manufactured crack-free nickel-based superalloy with synergistic strength and plasticity via grain refinement and striped oxides inhibition. Compos Part B Eng. 2025;291:112038. doi:10.1016/j.compositesb.2024.112038.
6. Tan Q, Liu K, Li J, Geng S, Sun L, Skuratov V. A review on cracking mechanism and suppression strategy of nickel-based superalloys during laser cladding. J Alloys Compd. 2024;1001:175164. doi:10.1016/j.jallcom.2024.175164.
7. Sui T, Zhang Y, Xiang S, Shi D. Effect of complex stress states on creep rupture life of nickel-based superalloys: mechanisms and modeling. Eng Fract Mech. 2025;314(1):110749. doi:10.1016/j.engfracmech.2024.110749.
8. Kvapilova M, Kral P, Dvorak J, Hutar P, Sklenicka V. Evaluation of high-temperature creep behaviour in cast GTD 111 nickel-based superalloy. Procedia Struct Integr. 2024;52:89–98. doi:10.1016/j.prostr.2023.12.009.

9. Mercer C, Soboyejo ABO, Soboyejo WO. Micromechanisms of fatigue crack growth in a forged Inconel 718 nickel-based superalloy. Mater Sci Eng A. 1999;270(2):308–22. doi:10.1016/S0921-5093(99)00214-2.
10. Xu Z, Cao L, Zhu Q, Guo C, Li X, Hu X, et al. Creep property of Inconel 718 superalloy produced by selective laser melting compared to forging. Mater Sci Eng A. 2020;794:139947. doi:10.1016/j.msea.2020.139947.
11. Zheng W, Zhu Y, Zhang Y, Huang A, Wang H, Zhang K. Research on heat treatment of nickel-based superalloys by laser powder bed fusion: a review. J Alloys Compd. 2025;1010(6):177522. doi:10.1016/j.jallcom.2024.177522.
12. Siddiqui NA, Muzamil M, Jamil T, Hussain G. Heat sources in wire arc additive manufacturing and their impact on macro-microstructural characteristics and mechanical properties—an overview. Smart Mater Manuf. 2025;3:100059. doi:10.1016/j.smmf.2024.100059.
13. Nan W, Ge L, He Z, Sun Z, Lu J. Powder spreading and spreadability in powder-based additive manufacturing: state of the art and perspectives. Powder Technol. 2025;449(5):120393. doi:10.1016/j.powtec.2024.120393.
14. Haines MP, Rielli VV, Primig S, Haghdadi N. Powder bed fusion additive manufacturing of Ni-based superalloys: a review of the main microstructural constituents and characterization techniques. J Mater Sci. 2022;57(30):14135–87. doi:10.1007/s10853-022-07501-4.
15. Clare AT, Mishra RS, Merklein M, Tan H, Todd I, Chechik L, et al. Alloy design and adaptation for additive manufacture. J Mater Process Technol. 2022;299(5):117358. doi:10.1016/j.jmatprotec.2021.117358.
16. Zhao Y, Ma Z, Yu L, Liu Y. New alloy design approach to inhibiting hot cracking in laser additive manufactured nickel-based superalloys. Acta Mater. 2023;247:118736. doi:10.1016/j.actamat.2023.118736.
17. He X, Zhang Y, Shi H, Gu J, Li C, Kadau K, et al. Influence of orientation and temperature on the fatigue crack growth of a nickel-based directionally solidified superalloy. Mater Sci Eng A. 2014;618:153–60. doi:10.1016/j.msea.2014.09.007.
18. Tan L, Yang XG, Shi DQ, Huang WQ, Lyu SQ, Fan YS. Effect of microstructure rafting on deformation behaviour and crack mechanism during high-temperature low-cycle fatigue of a Ni-based single crystal superalloy. Int J Fatigue. 2025;190:108619. doi:10.1016/j.ijfatigue.2024.108619.
19. Mo B, Li T, Shi F, Deng L, Liu W. Crack initiation and propagation within nickel-based high-temperature alloys during laser-based directed energy deposition: a review. Opt Laser Technol. 2024;179(6):111327. doi:10.1016/j.optlastec.2024.111327.
20. Hao Z, He Z, Nie Z, Li J, Ma Z, Guo Q. Effects of residual Laves phase on microstructural evolution and mechanical properties of wire arc additive manufactured GH4169 Ni-based superalloy. Mater Sci Eng A. 2024;914(5):147175. doi:10.1016/j.msea.2024.147175.
21. Li X, Hou Y, Cai W, Yu H, Wang X, Li F, et al. Study on crack behavior of GH3230 superalloy fabricated via high-throughput additive manufacturing. Materials. 2024;17(17):4225. doi:10.3390/ma17174225.
22. Wahlmann B, Leidel D, Markl M, Körner C. Numerical alloy development for additive manufacturing towards reduced cracking susceptibility. Crystals. 2021;11(8):902. doi:10.3390/cryst11080902.
23. Park JU, Jun SY, Lee BH, Jang JH, Lee BS, Lee HJ, et al. Alloy design of Ni-based superalloy with high γ' volume fraction suitable for additive manufacturing and its deformation behavior. Addit Manuf. 2022;52:102680. doi:10.1016/j.addma.2022.102680.
24. Markanday JFS. Applications of alloy design to cracking resistance of additively manufactured Ni-based alloys. Mater Sci Technol. 2022;38(16):1300–14. doi:10.1080/02670836.2022.2068759.
25. Horst OM, Adler D, Git P, Wang H, Streitberger J, Holtkamp M, et al. Exploring the fundamentals of Ni-based superalloy single crystal (SX) alloy design: chemical composition vs. microstructure. Mater Des. 2020;195(115):108976. doi:10.1016/j.matdes.2020.108976.
26. Liao P, Zhou GY, Zhang K, Ma H, Duan P, Zhang CC, et al. Phase diagram-guided composition design and property investigation of Ni-based filler metals. Mater Sci Eng A. 2024;891:145946. doi:10.1016/j.msea.2023.145946.
27. Liu Y, Xu B, Huangfu W, Yin H. Nickel-based polycrystalline superalloy composition design framework based on non-dominated sorting genetic algorithm II. Comput Mater Sci. 2023;220(2):112065. doi:10.1016/j.commatsci.2023.112065.

28. Xu G-H, Duan R, Wang L, Liu Y, Meng F-Q. Effect of compositional homogenization on hot workability of Ni-based GH4061 superalloy. Trans Nonferrous Met Soc China. 2023;33(6):1792–802. doi:10.1016/S1003-6326(23)66222-3.
29. Wang Y, Zhao M, Li Z, Li X, Yin F, He J. The synergistic effect of Re and W on the evolution of TCP phases in Nickel-based superalloys. J Alloys Compd. 2022;900(41):163286. doi:10.1016/j.jallcom.2021.163286.
30. Wei Q, Xie Y, Teng Q, Shen M, Sun S, Cai C. Crack types, mechanisms, and suppression methods during high-energy beam additive manufacturing of nickel-based superalloys: a review. Chin J Mech Eng Addit Manuf Front. 2022;1(4):100055. doi:10.1016/j.cjmeam.2022.100055.
31. Guo C, Li G, Li S. Additive manufacturing of Ni-based superalloys: residual stress, mechanisms of crack formation and strategies for crack inhibition. Nano Mater Sci. 2023;5(1):53–77. doi:10.1016/j.nanoms.2022.08.001.
32. Long H, Mao S, Liu Y, Zhang Z, Han X. Microstructural and compositional design of Ni-based single crystalline superalloys—a review. J Alloys Compd. 2018;743:203–20. doi:10.1016/j.jallcom.2018.01.224.
33. Zhang Y, Hu X, Li C, Xu W, Zhao Y. Composition design, phase transitions of a new polycrystalline Ni-Cr-Co-W base superalloy and its isothermal oxidation dynamics behaviors at 1300°C. Mater Des. 2017;129(1):26–33. doi:10.1016/j.matdes.2017.05.028.
34. Yu H, Fu J, Wang C, Chen Y, Wang L, Fang H, et al. Robust additive manufacturable Ni superalloys designed by the integrated optimization of local elemental segregation and cracking susceptibility criteria. Acta Mater. 2024;266:119658. doi:10.1016/j.actamat.2024.119658.
35. Pan P, Chen S, Zheng J, Xu C, Liu F, Li Z. Welding solidification cracking susceptibility and behavior of nickel based ERNiMo-2 wire. Mater Lett. 2022;314(12):131774. doi:10.1016/j.matlet.2022.131774.
36. Wall A, Benoit MJ. A review of existing solidification crack tests and analysis of their transferability to additive manufacturing. J Mater Process Technol. 2023;320(5):118090. doi:10.1016/j.jmatprotec.2023.118090.
37. Hu YL, Lin X, Yu XB, Xu JJ, Lei M, Huang WD. Effect of Ti addition on cracking and microhardness of Inconel 625 during the laser solid forming processing. J Alloys Compd. 2017;711(41):267–77. doi:10.1016/j.jallcom.2017.03.355.
38. Kadoi K, Matsumoto Y, Chiba H, Inoue H. Solidification cracking susceptibility of alloy 718 during additive manufacturing and evaluating method. J Mater Res Technol. 2024;33:6389–96. doi:10.1016/j.jmrt.2024.11.021.
39. Ren W, Lu F, Yang R, Liu X, Li Z. Liquation cracking in fiber laser welded joints of inconel 617. J Mater Process Technol. 2015;226(4):214–20. doi:10.1016/j.jmatprotec.2015.07.004.
40. Yang X, Liu M, Yu H, Liu Z, Li J, Xu W. The cracking behavior of Ni superalloys fabricated by laser directed energy deposition: the spatial distribution and formation mechanism. Mater Sci Eng A. 2025;924(8):147862. doi:10.1016/j.msea.2025.147862.
41. Ojo OA, Richards NL, Chaturvedi MC. Contribution of constitutional liquation of gamma prime precipitate to weld HAZ cracking of cast inconel 738 superalloy. Scr Mater. 2004;50(5):641–6. doi:10.1016/j.scriptamat.2003.11.025.
42. Li Y, Kang M, Zhou Y, Xu Y, Yu H, Pan Y, et al. Liquation cracking facilitated by stray-grain chains in a high-γ'-content nickel-based alloy K4002 produced via electron beam powder bed fusion. Mater Charact. 2024;218(1):114589. doi:10.1016/j.matchar.2024.114589.
43. Jeong HE, Seo SM, Chun EJ. Effect of local carbide formation behavior on repair weld liquation cracking susceptibility for long-term-serviced 247LC superalloy. J Mater Res Technol. 2024;28(10):110–22. doi:10.1016/j.jmrt.2023.12.003.
44. Chen Y, Lu F, Zhang K, Nie P, Elmi Hosseini SR, Feng K, et al. Dendritic microstructure and hot cracking of laser additive manufactured Inconel 718 under improved base cooling. J Alloys Compd. 2016;670:312–21. doi:10.1016/j.jallcom.2016.01.250.
45. Luu DN, Zhou W, Nai SML. Mitigation of liquation cracking in selective laser melted Inconel 718 through optimization of layer thickness and laser energy density. J Mater Process Technol. 2022;299:117374. doi:10.1016/j.jmatprotec.2021.117374.

46. Li Y, Long H, Wei B, Zhou J, Lin F. Multiple preheating processes for suppressing liquefaction cracks in IN738LC superalloy fabricated by electron beam powder bed fusion (EB-PBF). Materials. 2024;17(22):5667. doi:10.3390/ma17225667.
47. Roy I, Balikci E, Ibekwe S, Raman A. Precipitate growth activation energy requirements in the duplex size γ' distribution in the superalloy IN738LC. J Mater Sci. 2005;40(23):6207–15. doi:10.1007/s10853-005-3154-6.
48. Song Y, Zou Z, Li Y, Lu Y, Li H, Zhao G. Effect of temperature on dynamic strain aging and intermediate temperature embrittlement of nickel-based alloy N06625. Mater Today Commun. 2024;40:109796. doi:10.1016/j.mtcomm.2024.109796.
49. Newman RC, Healey C. Stability, validity, and sensitivity to input parameters of the slip-dissolution model for stress-corrosion cracking. Corros Sci. 2007;49(10):4040–50. doi:10.1016/j.corsci.2007.05.001.
50. Yoo SC, Choi KJ, Kim T, Kim SH, Kim JY, Kim JH. Microstructural evolution and stress-corrosion-cracking behavior of thermally aged Ni-Cr-Fe alloy. Corros Sci. 2016;111:39–51. doi:10.1016/j.corsci.2016.04.051.
51. Hwang SS, Kim HP, Lee DH, Kim UC, Kim JS. The mode of stress corrosion cracking in Ni-base alloys in high temperature water containing lead. J Nucl Mater. 1999;275(1):28–36. doi:10.1016/S0022-3115(99)00111-7.
52. Kuang W, Song M, Was GS. Insights into the stress corrosion cracking of solution annealed alloy 690 in simulated pressurized water reactor primary water under dynamic straining. Acta Mater. 2018;151:321–33. doi:10.1016/j.actamat.2018.04.002.
53. Yang X, Xu Y, Lu J, Huang J, Li W. Studying the formation of nodules in a Ni-Fe-Cr based superalloy used in fireside corrosion under the impact of creep stress. Corros Sci. 2024;234:112158. doi:10.1016/j.corsci.2024.112158.
54. Elsherkisi M, Duarte Martinez F, Mason-Flucke J, Gray S, Castelluccio GM. Interaction of stress corrosion cracks in single crystals Ni-Base superalloys. Eng Fract Mech. 2024;298:109899. doi:10.1016/j.engfracmech.2024.109899.
55. Nguyen TT, Bolivar J, Réthoré J, Baietto MC, Fregonese M. A phase field method for modeling stress corrosion crack propagation in a nickel base alloy. Int J Solids Struct. 2017;112(4):65–82. doi:10.1016/j.ijsolstr.2017.02.019.
56. Sato Y, Watanabe K, Shoji T. Simulation of stress corrosion cracking behavior in a tube-shaped specimen of nickel-based alloy 600. Nucl Eng Des. 2008;238(1):1–7. doi:10.1016/j.nucengdes.2007.06.009.
57. Arnoux P. Atomistic simulations of stress corrosion cracking. Corros Sci. 2010;52(4):1247–57. doi:10.1016/j.corsci.2009.12.024.
58. Bale H, Kothari M, Holwell A, Phaneuf M, Gray S, Legget J. Investigation of stress corrosion cracking in CMSX-4 turbine blade alloys using deep learning assisted X-ray microscopy. Microsc Microanal. 2022;28(S1):2052–3. doi:10.1017/S1431927622007942.
59. Volpe L, Burke MG, Scenini F. Correlation between grain boundary migration and stress corrosion cracking of alloy 600 in hydrogenated steam. Acta Mater. 2020;186(6):454–66. doi:10.1016/j.actamat.2020.01.020.
60. Nishikawa H, Habib K, Furuya Y, Hara T, Osada T, Kawagishi K. Short fatigue crack growth mechanism in Ni-Co based superalloy at elevated temperatures and in oxidative atmospheres. Mater Sci Eng A. 2023;885:145655. doi:10.1016/j.msea.2023.145655.
61. Rai RK. The role of cyclic oxidation on low cycle fatigue crack initiation and growth behaviour of a Ni-based superalloy. Mater Chem Phys. 2025;332:130311. doi:10.1016/j.matchemphys.2024.130311.
62. Wu CH, Jiang R, Zhang LC, Wang YC, Chen Y, Song YD. Oxidation accelerated dwell fatigue crack growth mechanisms of a coarse grained PM Ni-based superalloy at elevated temperatures. Corros Sci. 2022;209(4):110702. doi:10.1016/j.corsci.2022.110702.
63. Park S, Tanaka Y, Okazaki S, Funakoshi Y, Kawashima H, Matsunaga H. Role of grain boundaries and precipitates in small, fatigue crack-growth resistance of additively-manufactured, Ni-based superalloy 718 under torsional cyclic loading. Mater Lett. 2023;350:134844. doi:10.1016/j.matlet.2023.134844.
64. Kim D, Jiang R, Evangelou A, Sinclair I, Reed PAS. Effects of γ' size and carbide distribution on fatigue crack growth mechanisms at 650°C in an advanced Ni-based superalloy. Int J Fatigue. 2021;145:106086. doi:10.1016/j.ijfatigue.2020.106086.
65. Escobar-Moreno I, Nieto-Valeiras E, LLorca J. Slip transfer and crack initiation at grain and twin boundaries during strain-controlled fatigue of solution-hardened Ni-based alloys. Acta Mater. 2025;283(1):120497. doi:10.1016/j.actamat.2024.120497.

66. Zhang M, Zhang Y, Liu H, Zou Q. Judgment criterion of the dominant factor of creep-fatigue crack growth in a nickel-based superalloy at elevated temperature. Int J Fatigue. 2019;118:176–84. doi:10.1016/j.ijfatigue.2018.09.007.
67. Piard A, Gamby D, Carbou C, Mendez J. A numerical simulation of creep-fatigue crack growth in nickel-base superalloys. Eng Fract Mech. 2004;71(16–17):2299–2317. doi:10.1016/j.engfracmech.2004.02.002.
68. Yang H, Bao R, Zhang J, Peng L, Fei B. Creep-fatigue crack growth behaviour of a nickel-based powder metallurgy superalloy under high temperature. Eng Fail Anal. 2011;18(3):1058–66. doi:10.1016/j.engfailanal.2010.12.025.
69. Li KS, Cheng LY, Xu Y, Wang RZ, Zhang Y, Zhang XC, et al. A dual-scale modelling approach for creep-fatigue crack initiation life prediction of holed structure in a nickel-based superalloy. Int J Fatigue. 2022;154(19):106522. doi:10.1016/j.ijfatigue.2021.106522.
70. Shlyannikov V, Sulamanidze A, Kosov D. Crack growth analysis of XH73M nickel alloy under fatigue, creep-fatigue interaction and thermo-mechanical conditions. Procedia Struct Integr. 2024;52(1):214–23. doi:10.1016/j.prostr.2023.12.022.
71. Lv P, Liu L, Ge C, Zhao Y, Zhang J. Stress sensitivity and its influence on high-temperature creep behavior of a novel 2nd-generation low-cost nickel based single crystal superalloy. Mater Sci Eng A. 2024;915(1):147187. doi:10.1016/j.msea.2024.147187.
72. Yin Q, Wang JD, Wen ZX, Shi QY, Lian YD, Yue ZF. Creep-fatigue behavior of nickel-based single crystal superalloy with different orientations: experimental characterization and multi-scale simulation. Mater Sci Eng A. 2023;886:145667. doi:10.1016/j.msea.2023.145667.
73. Kou S. A criterion for cracking during solidification. Acta Mater. 2015;88(11):366–74. doi:10.1016/j.actamat.2015.01.034.
74. Singer ARE, Jennings PH. Hot-shortness of the aluminium-silicon alloys of commercial purity. J Inst Met. 1946;73:197–212.
75. DuPont JN, Lippold JC, Kiser SD. Precipitation-Strengthened Ni-base Alloys. In: Welding metallurgy and weldability of nickel-base alloys. 2009. p. 157–254. doi:10.1002/9780470500262.ch4.
76. Clyne B, Davies G. The influence of composition on solidification cracking susceptibility in binary alloys. Br Foundrymen. 1981;74:65–73.
77. Huron ES, Reed RC, Hardy MC, Mills MJ, Montero RE. Superalloys 2012. Hoboken, NJ, USA: John Wiley & Sons, Inc.; 2012. doi:10.1002/9781118516430.
78. Tang YT, Panwisawas C, Ghoussoub JN, Gong Y, Clark JWG, Németh AAN, et al. Alloys-by-design: application to new superalloys for additive manufacturing. Acta Mater. 2021;202(3):417–36. doi:10.1016/j.actamat.2020.09.023.
79. Kaplan B. A comprehensive model for quantitatively predicting the comparative strain-age cracking risk in welded or additively manufactured Ni-base superalloys. Mater Today Commun. 2024;40(16):109408. doi:10.1016/j.mtcomm.2024.109408.
80. Harrison NJ. Selective laser melting of nickel superalloys: solidification, microstructure and material response [Ph.D. thesis]. Sheffield, UK: University of Sheffield; 2016.
81. Chandra S, Tan X, Narayan RL, Wang C, Tor SB, Seet G. A generalised hot cracking criterion for nickel-based superalloys additively manufactured by electron beam melting. Addit Manuf. 2021;37:101633. doi:10.1016/j.addma.2020.101633.
82. Rappaz M, Drezet JM, Gremaud M. A new hot-tearing criterion. Metall Mater Trans A. 1999;30(2):449–55. doi:10.1007/s11661-999-0334-z.
83. Xu J. High-performance nickel-based superalloys for additive manufacturing [Internet]. Vol. 2217. Linköping, Sweden: Linköping University Electronic Press; 2022 [cited 2025 Mar 7]. Available from: http://urn.kb.se/resolve?urn=urn:nbn:se:liu:diva-184161.
84. Clyne B, Davies G. A quantitative solidification cracking test for castings and an evaluation of cracking in aluminium–magnesium alloys. Br Foundrymen. 1975;68:238–44.
85. Zhang Y, Cao B, Liu Z, Jiang D, Ye S, Liu T, et al. Inhibiting cracking and improving strength-ductility for laser powder bed fusion René 104 superalloy by Sc and Y microalloying. Mater Sci Eng A. 2024;913:147054. doi:10.1016/j.msea.2024.147054.

86. Zhang X, Mu Y, Lu N, Li Q, Chen S, Zhou Y, et al. Effect of solid solution elements on cracking susceptibility of Ni-based superalloys during additive manufacturing. J Mater Sci Technol. 2024;190:218–28. doi:10.1016/j.jmst.2023.11.073.
87. Yu H, Liang J, Bi Z, Li J, Xu W. Computational design of novel Ni superalloys with low crack susceptibility for additive manufacturing. Metall Mater Trans A. 2022;53(6):1945–54. doi:10.1007/s11661-022-06653-x.
88. Liu Z, Han Q, Zhang Z, Wang L, Ma T, Gao Z, et al. Design of a novel crack-free precipitation-strengthened nickel-based superalloy and composites for laser powder bed fusion. Virtual Phys Prototyp. 2023;18(1):e2224769. doi:10.1080/17452759.2023.2224769.
89. Chen M, Hua L, Hu Z, Dong K, Qin X. Cracking and suppression mechanisms of directed energy deposited IN738 superalloy revealed by microstructural characterization, *in-situ* thermal monitoring, and numerical simulations. J Alloys Compd. 2025;1020:179446. doi:10.1016/j.jallcom.2025.179446.
90. Xu J, Kontis P, Peng RL, Moverare J. Modelling of additive manufacturability of nickel-based superalloys for laser powder bed fusion. Acta Mater. 2022;240:118307. doi:10.1016/j.actamat.2022.118307.
91. Harrison NJ, Todd I, Mumtaz K. Reduction of micro-cracking in nickel superalloys processed by Selective Laser Melting: a fundamental alloy design approach. Acta Mater. 2015;94(1):59–68. doi:10.1016/j.actamat.2015.04.035.
92. Tanaka K, Mura T. A dislocation model for fatigue crack initiation. J Appl Mech. 1981;48(1):97–103. doi:10.1115/1.3157599.
93. Liu X, Lu S. A micro-crack initiation life simulation method by improving the Tanaka-Mura's model of slip behavior. Int J Fatigue. 2021;145:106108. doi:10.1016/j.ijfatigue.2020.106108.
94. Cui P, Liu Z, Zhao J, Ren X. Correlation between surface integrity and low cycle fatigue life of machined inconel 718. Metals. 2024;14(2):178. doi:10.3390/met14020178.
95. Zou T, Liu M, Wang Q, Jiang Y, Wu H, Gao Z, et al. Evolutionary mechanisms in the plastic deformation of γ'-Ni3(Al, Ti)-strengthened additively manufactured nickel-based 939 superalloys at intermediate temperatures. Mater Des. 2024;239(6):112795. doi:10.1016/j.matdes.2024.112795.
96. Xu Y, Zhang L, Li J, Xiao X, Cao X, Jia G, et al. Relationship between Ti/Al ratio and stress-rupture properties in nickel-based superalloy. Mater Sci Eng A. 2012;544:48–53. doi:10.1016/j.msea.2012.03.006.
97. Zhang F, Zhou L, Xie X, Zhang Z, Chao Q, Fan G. Crack inhibition and crystallographic texture control in an additively manufactured IN738LC Ni-based superalloy. J Mater Res Technol. 2024;33(4):652–66. doi:10.1016/j.jmrt.2024.09.101.
98. Ryou K, Ji Im H, Park J, Choi PP. Microstructural evolution and hot cracking prevention in direct-laser-deposited Ni-based superalloy through Hf addition. Mater Des. 2023;234(1):112298. doi:10.1016/j.matdes.2023.112298.
99. Wu S, Chia HY, Zhang T, Jia Y, Mu Y, Zhang Q, et al. A precipitation strengthened high entropy alloy with high (Al+Ti) content for laser powder bed fusion: synergizing in trinsic hot cracking resistance and ultrahigh strength. Acta Mater. 2023;258:119193. doi:10.1016/j.actamat.2023.119193.
100. Liu Y, Wu D, Gao Z, Gong X, Shao Y, Cao Y, et al. Influence of cold metal transfer welding parameters on the welding hot crack of Mar-M247 nickel-based superalloy. J Mater Res Technol. 2024;30:6341–54. doi:10.1016/j.jmrt.2024.05.061.
101. Zhao G, Zang X, Qi F. Effect of boron on isothermal oxidation behavior of a nickel-base superalloy with high Al and Ti contents. J Alloys Compd. 2020;846:156490. doi:10.1016/j.jallcom.2020.156490.
102. Wang H, Yang J, Meng J, Ci S, Yang Y, Sheng N, et al. Effects of B content on microstructure and high-temperature stress rupture properties of a high chromium polycrystalline nickel-based superalloy. J Alloys Compd. 2021;860(1):157929. doi:10.1016/j.jallcom.2020.157929.
103. Li X, Ou M, Wang M, Zha X, Ma Y, Liu K. Microstructure evolution and stress rupture properties of K4750 alloys with various B contents during long-term aging. J Mater Sci Technol. 2021;73:108–15. doi:10.1016/j.jmst.2020.10.014.
104. Després A, Antonov S, Mayer C, Tassin C, Veron M, Blandin JJ, et al. On the role of boron, carbon and zirconium on hot cracking and creep resistance of an additively manufactured polycrystalline superalloy. Materialia. 2021;19(8):101193. doi:10.1016/j.mtla.2021.101193.
105. Mostafaei M, Abbasi SM. Influence of Zr content on the incipient melting behavior and stress-rupture life of CM247 LC nickel base superalloy. J Alloys Compd. 2015;648:1031–7. doi:10.1016/j.jallcom.2015.07.104.

106. Tsai YL, Wang SF, Bor HY, Hsu YF. Effects of Zr addition on the microstructure and mechanical behavior of a fine-grained nickel-based superalloy at elevated temperatures. Mater Sci Eng A. 2014;607:294–301. doi:10.1016/j.msea.2014.03.136.
107. Zhou Y, Wang B, Li S, Li W, Xu K, Liang J, et al. On the segregation behavior and influences of minor alloying element Zr in nickel-based superalloys. J Alloys Compd. 2022;897:163169. doi:10.1016/j.jallcom.2021.163169.
108. Zhao Y, Guo Q, Li C, Yang Z, Zhang J, Huang Y, et al. Achieving superior elevated temperature properties in additive manufactured nickel-based superalloys through unique alloy design. Addit Manuf. 2024;88(10):104273. doi:10.1016/j.addma.2024.104273.
109. Liu S, Ye XX, Ming C, Yan S, Jiang L, Li Z, et al. An approach to improve the oxidation resistance of a Ni-28W-6Cr alloy by hindering the oxygen vacancy-mediated oxidation. Corros Sci. 2021;187:109480. doi:10.1016/j.corsci.2021.109480.
110. Zhang J, Singer RF. Effect of Zr and B on castability of Ni-based superalloy IN792. Metall Mater Trans A. 2004;35(4):1337–42. doi:10.1007/s11661-004-0308-0.
111. Ning T, Guoqi Z, Tai M, Sugui T, Lirong L, Huajin Y, et al. Ultra-high-temperature creep behavior of a single-crystal nickel-based superalloy containing 6% Re/5% Ru. Mater Charact. 2021;180(2):111394. doi:10.1016/j.matchar.2021.111394.
112. Tian S, Wu J, Shu D, Su Y, Yu H, Qian B. Influence of element Re on deformation mechanism within γ' phase of single crystal nickel-based superalloys during creep at elevated temperatures. Mater Sci Eng A. 2014;616:260–7. doi:10.1016/j.msea.2014.08.001.
113. Zhang J, Zong H, Lu F, Huang T, Wang D, Zhang J, et al. Synergistic effects of Re and Ta on the distribution of W in Ni-based superalloys. Intermetallics. 2022;147:107609. doi:10.1016/j.intermet.2022.107609.
114. Zhao G, Tian S, Zhang S, Tian N, Liu L. Deformation and damage features of a Re/Ru-containing single crystal nickel base superalloy during creep at elevated temperature. Prog Nat Sci Mater Int. 2019;29(2):210–6. doi:10.1016/j.pnsc.2019.01.013.
115. Li X, Huang M, Zhao L, Liang S, Zhu Y, Li Z. Study of Re strengthening mechanisms in nickel-based superalloy. Intermetallics. 2024;167:108209. doi:10.1016/j.intermet.2024.108209.
116. Ding Q, Li S, Chen LQ, Han X, Zhang Z, Yu Q, et al. Re segregation at interfacial dislocation network in a nickel-based superalloy. Acta Mater. 2018;154:137–46. doi:10.1016/j.actamat.2018.05.025.
117. Ryou K, Yoo B, Choi PP. On the oxygen-induced hot cracking in a direct laser deposited Ni-based superalloy. Scr Mater. 2021;196:113751. doi:10.1016/j.scriptamat.2021.113751.
118. Qiu C, Chen H, Liu Q, Yue S, Wang H. On the solidification behaviour and cracking origin of a nickel-based superalloy during selective laser melting. Mater Charact. 2019;148:330–44. doi:10.1016/j.matchar.2018.12.032.
119. Xu J, Lin X, Guo P, Dong H, Wen X, Li Q, et al. The initiation and propagation mechanism of the overlapping zone cracking during laser solid forming of IN-738LC superalloy. J Alloys Compd. 2018;749:859–70. doi:10.1016/j.jallcom.2018.03.366.
120. Messé OMDM, Muñoz-Moreno R, Illston T, Baker S, Stone HJ. Metastable carbides and their impact on recrystallisation in IN738LC processed by selective laser melting. Addit Manuf. 2018;22:394–404. doi:10.1016/j.addma.2018.05.030.
121. Ma Q, Li X, Xin R, Liu E, Gao Q, Sun L, et al. Thermodynamic calculation and machine learning aided composition design of new nickel-based superalloys. J Mater Res Technol. 2023;26:4168–78. doi:10.1016/j.jmrt.2023.08.139.
122. Wu D, Han Q, Wu M, Zhang H, Wang Y, Lu K, et al. Laser powder bed fusion of a composition-modified IN738 alloy based on thermodynamic calculations. Mater Sci Eng A. 2025;922(6):147605. doi:10.1016/j.msea.2024.147605.
123. Mukherjee T, Shinjo J, DebRoy T, Panwisawas C. Integrated modeling to control vaporization-induced composition change during additive manufacturing of nickel-based superalloys. npj Comput Mater. 2024;10(1):230. doi:10.1038/s41524-024-01418-z.
124. Xie J. Prospects of materials genome engineering frontiers. Mater Genome Eng Adv. 2023;1(2):e17. doi:10.1002/mgea.17.

125. Xu J, Li L, Liu X, Li H, Feng Q. Fast characterization framework for creep microstructure of a nickel-based SX superalloy with high-throughput experiments and deep learning methods. Mater Charact. 2022;187(12):111857. doi:10.1016/j.matchar.2022.111857.
126. Vecchio KS. High-throughput (HTP) synthesis: updated high-throughput rapid experimental alloy development (HT-READ). Curr Opin Solid State Mater Sci. 2024;31(6477):101164. doi:10.1016/j.cossms.2024.101164.
127. Yang C, You X, Yu R, Xu Y, Zhang J, Fan X, et al. Semi-supervised deep transfer learning for the microstructure recognition in the high-throughput characterization of nickel-based superalloys. Mater Charact. 2023;203(10):113094. doi:10.1016/j.matchar.2023.113094.
128. Wang MX, Zhu H, Yang GJ, Liu K, Li JF, Kong LT. Solid-solution strengthening effects in binary Ni-based alloys evaluated by high-throughput calculations. Mater Des. 2021;198(7):109359. doi:10.1016/j.matdes.2020.109359.
129. Ouyang G, Palasyuk O, Singh P, Ray PK, Deodeshmukh V, Cui J, et al. Predictive design of novel nickel-based superalloys beyond Haynes 282. Acta Mater. 2024;275:120045. doi:10.1016/j.actamat.2024.120045.
130. Vecchio KS, Dippo OF, Kaufmann KR, Liu X. High-throughput rapid experimental alloy development (HT-READ). Acta Mater. 2021;221:117352. doi:10.1016/j.actamat.2021.117352.
131. Inayathullah S, Buddala R. Review of machine learning applications in additive manufacturing. Results Eng. 2025;25:103676. doi:10.1016/j.rineng.2024.103676.
132. Liu Y, Wu J, Wang Z, Lu XG, Avdeev M, Shi S, et al. Predicting creep rupture life of Ni-based single crystal superalloys using divide-and-conquer approach based machine learning. Acta Mater. 2020;195(2):454–67. doi:10.1016/j.actamat.2020.05.001.
133. Xu B, Yin H, Jiang X, Zhang C, Zhang R, Wang Y, et al. Computational materials design: composition optimization to develop novel Ni-based single crystal superalloys. Comput Mater Sci. 2022;202(12):111021. doi:10.1016/j.commatsci.2021.111021.
134. Liu Y, Zhao T, Ju W, Shi S. Materials discovery and design using machine learning. J Materiomics. 2017;3(3):159–77. doi:10.1016/j.jmat.2017.08.002.
135. Li K, Zhan J, Wang Y, Qin Y, Gong N, Zhang DZ, et al. Application of data-driven methods for laser powder bed fusion of Ni-based superalloys: a review. J Manuf Process. 2025;133(625):285–321. doi:10.1016/j.jmapro.2024.11.053.
136. Tan L, Yang XG, Shi DQ, Hao WQ, Fan YS. Unified fatigue life modelling and uncertainty estimation of Ni-based superalloy family with a supervised machine learning approach. Eng Fract Mech. 2022;275:108813. doi:10.1016/j.engfracmech.2022.108813.
137. Deng Y, Zhang Y, Gong X, Hu W, Wang Y, Liu Y, et al. An intelligent design for Ni-based superalloy based on machine learning and multi-objective optimization. Mater Des. 2022;221(8):110935. doi:10.1016/j.matdes.2022.110935.
138. Yu H, Zhao Q, Fu J, Hu Y, Liang J, Li J, et al. The design of oxidation resistant Ni superalloys for additive manufacturing. Addit Manuf. 2025;97:104616. doi:10.1016/j.addma.2024.104616.
139. Gao J, Tong Y, Zhang H, Zhu L, Hu Q, Hu J, et al. Machine learning assisted design of Ni-based superalloys with excellent high-temperature performance. Mater Charact. 2023;198:112740. doi:10.1016/j.matchar.2023.112740.
140. Awd M, Saeed L, Walther F. A review on the enhancement of failure mechanisms modeling in additively manufactured structures by machine learning. Eng Fail Anal. 2023;151:107403. doi:10.1016/j.engfailanal.2023.107403.